JOURNAL OF VIROLOGY, May 2005, p. 5337–5345 Vol. 79, No. 9
0022-538X/05/$08.00+0 doi:10.1128/JVI.79.9.5337–5345.2005
Copyright © 2005, American Society for Microbiology. All Rights Reserved.

Structure and Assembly of a $T=1$ Virus-Like Particle in BK Polyomavirus

Josefina Nilsson,[1] Naoyuki Miyazaki,[1] Li Xing,[1] Bomu Wu,[1] Lena Hammar,[1] Tian Cheng Li,[2] Naokazu Takeda,[2] Tatsuo Miyamura,[2] and R. Holland Cheng[1,3]*

Department of Biosciences at Novum, Karolinska Institute, 14157 Huddinge, Sweden[1]; Department of Virology II, National Institute of Infectious Diseases, Tokyo 162-8640, Japan[2]; and Molecular and Cellular Biology, University of California, Davis, California 95616[3]

Received 27 July 2004/Accepted 7 December 2004

In polyomaviruses the pentameric capsomers are interlinked by the long C-terminal arm of the structural protein VP1. The $T=7$ icosahedral structure of these viruses is possible due to an intriguing adaptability of this linker arm to the different local environments in the capsid. To explore the assembly process, we have compared the structure of two virus-like particles (VLPs) formed, as we found, in a calcium-dependent manner by the VP1 protein of human polyomavirus BK. The structures were determined using electron cryomicroscopy (cryo-EM), and the three-dimensional reconstructions were interpreted by atomic modeling. In the small VP1 particle, 26.4 nm in diameter, the pentameric capsomers form an icosahedral $T=1$ surface lattice with meeting densities at the threefold axes that interlinked three capsomers. In the larger particle, 50.6 nm in diameter, the capsomers form a $T=7$ icosahedral shell with three unique contacts. A folding model of the BKV VP1 protein was obtained by alignment with the VP1 protein of simian virus 40 (SV40). The model fitted well into the cryo-EM density of the $T=7$ particle. However, residues 297 to 362 of the C-terminal arm had to be remodeled to accommodate the higher curvature of the $T=1$ particle. The loops, before and after the C-terminal short helix, were shown to provide the hinges that allowed curvature variation in the particle shell. The meeting densities seen at the threefold axes in the $T=1$ particle were consistent with the triple-helix interlinking contact at the local threefold axes in the $T=7$ structure.

The BK virus (BKV) is a human virus belonging to the *Polyomaviridae* family. It is a nonenveloped virus (~50.0 nm in diameter) with a circular double-stranded DNA genome (~5 kb). The capsid has icosahedral symmetry and is built of 72 capsomers that are all pentamers of the protein VP1 arranged in a $T=7$ icosahedral lattice (21). All known polyomaviruses have three structural proteins (VP1, VP2, and VP3), of which VP1 is the major capsid protein. Overall amino acid sequence homology between BKV and the other human polyomavirus, JCV, is 75%, and that with the simian polyomavirus (SV40) is 69% (9). In the VP1 protein the sequence similarity rises to 77% and 74% for the JCV and SV40, respectively (35). Due to the high similarity, the solved atomic structure of VP1 of SV40 provides us a template to create a model of the BKV VP1 protein folding.

The structures of the SV40 and murine polyomavirus have been determined and show similar features to that seen in the BKV (1, 12). The VP1 pentamer of SV40 and murine polyomavirus is built as a ring of five β-barrel-shaped VP1 monomers, tightly linked by interacting loops between the framework of β-strands (22, 33, 34, 40). The C-terminal subdomain of each VP1 monomer "invades" a neighboring pentamer, thereby tying the pentamers together in the virion shell. There are six unique monomers building up the capsid (monomer α, α′, and α″ at the local threefold; β, β′ around the icosahedral threefold, and γ at the twofold) (34). The major structural differences between the six unique monomers are found in their C termini and are essential for the formation of the icosahedral capsid. The most flexible region seemed to be the outermost C terminus of the peptide chain (amino acids 355 to 364). The structure of this region has not been defined in three of the six unique monomers (α, α″, and β).

Under certain conditions the polyomavirus capsid disassembles into pentamers, which can be reassembled. The reassembled particle may have different configurations and sizes depending on the buffer conditions. This was shown for recombinant SV40 VLPs (17) and recombinant murine polyoma VLPs (28, 29). In the latter case, Salunke et al. (29) demonstrated that three differently sized VLPs appeared, depending on the buffer conditions. They concluded through computational modeling that two of the reassembled murine polyomavirus particles had icosahedral symmetry and were composed of 12 and 72 pentamers, in a $T=1$ and $T=7$, respectively, surface lattice. The third particle was composed of 24 pentamers with an octahedral symmetry.

Many studies have demonstrated that calcium ions play an important role in viral assembly (3, 5, 6, 13, 14, 17, 20, 25, 26, 28). Besides the calcium-binding site, disulfide bonds have also been found to be involved in maintaining capsid stability of the polyomavirus (5, 6, 11, 14, 15, 19, 30, 36). Interpentameric disulfide linkages have been revealed by X-ray crystallography in the capsid structure of SV40 and murine polyomavirus (22, 33, 34).

* Corresponding author. Mailing address: Department of Molecular and Cellular Biology, University of California, Davis, CA 95616. Phone: (530) 752-3611. Fax: (530) 752-3085. E-mail: rhch@ucdavis.edu.

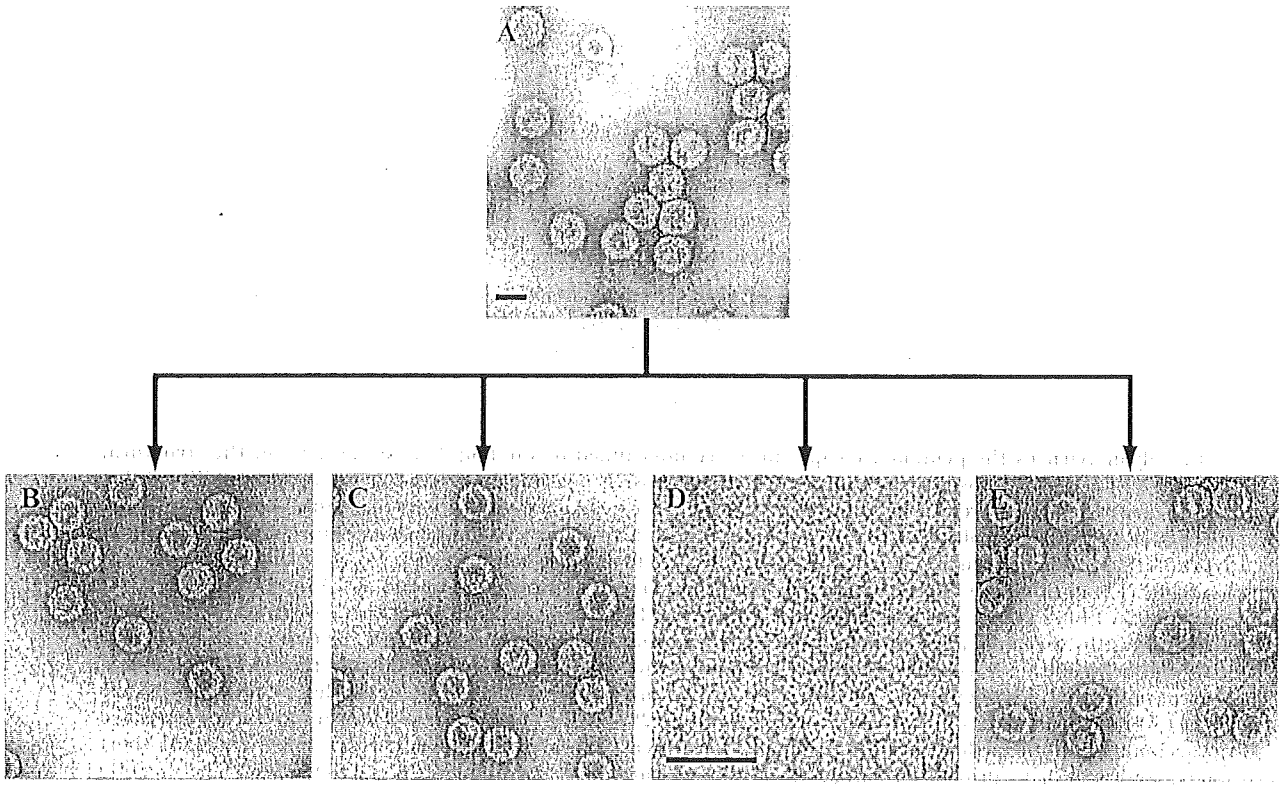

FIG. 1. Factors guiding disassembly of BKV VLPs. (A) Electron micrograph (negative stained) of recombinant BKV VLPs (0.5 mg/ml). To find dissociation conditions, the BKV VLPs (A) were equilibrated by dialysis against different concentrations of EDTA (10 to 100 mM), 2-ME (10 to 100 mM), and NaCl (0.15 to 1 M). All experiments were done overnight at room temperature, and the resulting appearance of the samples are shown in the electron micrographs B to E (negative stain). (B) Result from dialysis against 20 mM EDTA. (C) Result from dialysis against 30 mM 2-ME. (D) Result from dialysis against 20 mM EDTA and 30 mM 2-ME. (E) Result from dialysis against 20 mM EDTA, 30 mM 2-ME, and 0.6 M NaCl. Bars, 50 nm.

The gene of the major structural protein of the BKV VP1 was recently expressed in Tn5 cells using a recombinant baculovirus vector (21). The BKV VP1 self-assembled into VLPs in the nucleus, and the particles were then efficiently released into the culture medium. These VLPs possessed similar antigenicity as native BKV particles and were indistinguishable as negative-stained specimens in electron microscopy. The structure was determined to 2.0 nm resolution, using electron cryomicroscopy (cryo-EM) and three-dimensional reconstruction, and showed similar features to both SV40 and murine polyomavirus.

Here, we report for the first time the three-dimensional structure of a smaller BKV VLP determined by cryo-EM, image reconstruction, and docking of the VP1 model. We compare the structure of the two different BKV VLPs and explore the in vitro disassembly/reassembly process of them.

MATERIALS AND METHODS

Expression and purification of the BKV capsid protein VP1. For the large-scale expression of the BKV capsid protein VP1 (21, 37), an insect cell line from *Trichoplusia ni*, BTI-Tn 5B1-4 (Tn5) (Invitrogen, San Diego, CA) was used. Tn5 cells were infected with recombinant baculoviruses at a multiplicity of infection (MOI) of 10 and were incubated in EX-CELL 405 medium (JRH Biosciences, Lenexa, KS) for 7 days at 26.5°C. Intact cells, cell debris, and progeny baculoviruses were removed by centrifugation at 10,000 × *g* for 90 min. The supernatant was then spun at 25,000 rpm for 2 h in a Beckman SW28 rotor. The resulting pellet was resuspended in 4.5 ml of EX-CELL 405 at 4°C overnight. After mixing

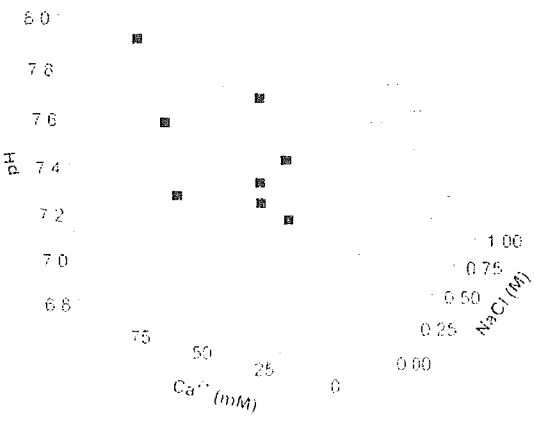

FIG. 2. Effect of buffer composition on the shape of reassembled particles. When the VLPs had been dissociated, the sample (now containing free pentamers) was dialyzed again against buffers with different concentrations of a monovalent salt, NaCl (0.0 to 1.0 M), pH (7.0 to 7.8), and a divalent ion, Ca^{2+} (0.0 to 100.0 mM). Square: buffer conditions when less then 30% of the reassembled particles had a $T = 1$ symmetry. Triangle: buffer conditions when more then 80% of the reassembled particles had a $T = 1$ symmetry. All experiments were done at room temperature and overnight.

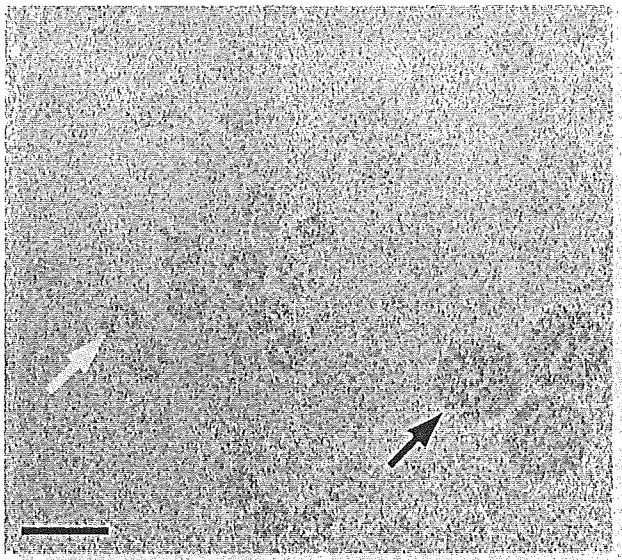

FIG. 3. Cryo-electron micrograph of BKV VLPs that were reassembled after overnight equilibration against 5 mM Ca^{2+}, 150 mM NaCl, and 10 mM Tris-HCl, pH 7.4. Two populations of BKV VLPs that differed in size can be seen (white arrow, small VLP; black arrow, large native-size VLP). Bar, 50 nm.

with 2.1 g of CsCl, the sample was centrifuged at 35,000 rpm for 24 h at 4°C in a Beckman SW50.1 rotor. Four bands were harvested by puncturing the tubes with a 22-gauge needle. To remove the CsCl, each band was diluted 10× and centrifuged for 2 h in a Beckman TLA55 rotor at 50,000 rpm; the pellet was then resuspended in 150 mM NaCl, 10 mM TRIS-HCl, pH 7.4.

Dialysis experiments. To screen for factors effecting dissociation and reassembly of the BKV VLPs, a homemade dialysis equipment that allowed dialyses of small amounts of sample (20 to 40 μl) was used. BKV VLPs (35 μl, 0.5 mg/ml) were first dialyzed against different concentrations of EDTA (10 to 100 mM), 2-mercaptoethanol (2-ME) (10 to 100 mM), and NaCl (0.15 to 1 M) in an attempt to dissociate the VLPs. When the VLPs had been dissociated, the sample (now containing free pentamers) was again dialyzed against buffers with different concentrations of a monovalent salt, NaCl (0.0 to 1.0 M), pH (7.0 to 7.8), and a divalent ion, Ca^{2+} (0.0 to 100.0 mM), to make the pentamers reassemble into VLPs. All experiments were done in room temperature and overnight. The selection of conditions for the second dialysis, like combinations of different pH, calcium, and NaCl concentrations, was done with the aid of the software DESIGN (32).

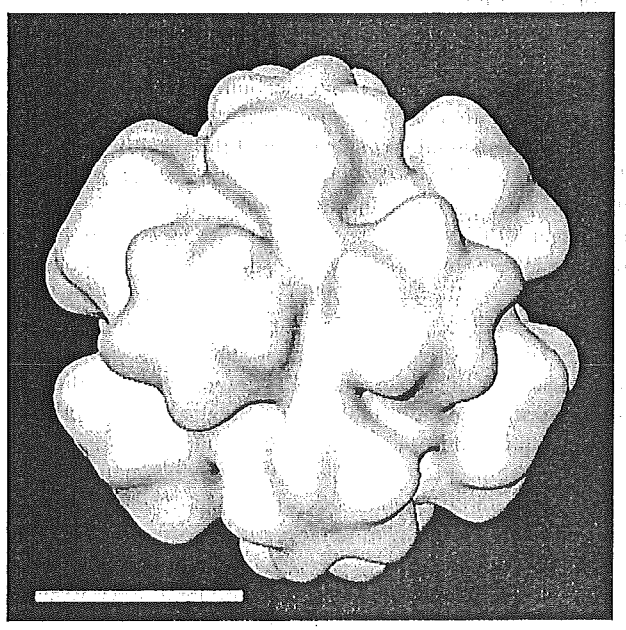

FIG. 4. Cryo-EM three-dimensional reconstruction of the small BKV VLP from Fig. 3. The particle is viewed along the twofold axis. It has icosahedral symmetry, and the VP1 protein establishes an arrangement according to a $T=1$ lattice with protruding capsomer at each fivefold. Bar, 10 nm.

To determine the proportion of small (26.4 nm in diameter) and large VLPs (50.6 nm in diameter) in the different reassembly experiments, samples were applied to carbon-coated grids, negatively stained, and checked by EM. Thirty fields were randomly chosen from each grid and micrograph taken. In each the numbers of small and large VLPs were counted.

Negative contrasting electron microscopy. For EM, a sample of ~3 μl was applied to the charged grid and allowed to settle for 20 seconds. The solution was removed by blotting with a filter paper and the sample washed once with 3 μl of water for 15 seconds before stained with a 2% uranyl acetate solution. After 15 seconds the uranyl acetate solution was blotted off with a filter paper. The samples were observed by a Philips CM120 electron microscope.

Cryo-electron microscopy and three-dimensional image analysis. Frozen-hydrated specimens were prepared by applying 3.0-μl droplets of an aqueous mixture of reassembled BKV VLPs (1.0 to 1.5 mg/ml) on 300-mesh copper grids coated with holey carbon film. The images of the frozen VLPs were recorded with a Philips CM120 (Philips Electronics Instruments) by defined low-dose condition. The micrographs were taken with Kodak SO163 films (Eastman Kodak Co., New York, NY) at 45,000 nominal magnifications and 120 kV operating voltage. Each area of specimen was recorded twice as focal pairs with defocus value of 1.0 and 3.0 μm, respectively (38). Micrographs with sufficiently separated and well-distributed particles, exhibiting minimal astigmatism, were digitized at 14-μm intervals (0.311-nm sampling at the specimen) with a Zeiss microdensitometer. Individual particle images were extracted and analyzed with icosahedral symmetry processing procedures to reconstruct the three-dimensional structure (39). Computations were performed with interactive FORTRAN programs on Alphastations (Digital Equipment Co., MA).

The initial phase origins of selected particle images were obtained by using a cross-correlation method, where the particle orientations were determined through modified self-common-lines and polar Fourier transform procedures (2, 10). This was followed by interparticle orientation refinement with increasing numbers of unique images by cross-common-lines procedures. To improve the sensitivity and reliability of the orientation refinement procedures with the BKV VLPs images, the data were Fourier-filtered to remove both low- and high-frequency noise beyond the processing regions. Refinement of origins and orientations was repeated in cycles at progressively higher spatial frequencies until no further improvement was found in the common-lines phase residues. Besides the procedures described above, back-projection images of the preliminary reconstruction were used as references to accurately refine the phase origins and orientations of the corresponding images. The resolution was progressively improved and the final three-dimensional reconstruction was computed to a resolution of 2.4 nm, which was within the limit imposed by the first zero of the contrast transfer function of the electron microscope.

Fitting of BKV VP1 model into the EM density map. The atomic model of BK VP1 protein was constructed from SV40 VP1 using the SWISS-MODEL Protein Modeling Server (31) and the software modeler. Following that, the fitting of the pentameric structures to the cryo-EM map of the $T=1$ particle was performed manually using O (16) based on one of the pentamers from the BKV $T=7$ capsid. We used the VP1 pentameric model of BKV at the pentavalent position in the $T=7$ particles to build the atomic model of the $T=1$ particles. For the initial fitting, only the core of the VP1 was used, which consists of residues 16 to 296. This was based on the fact that the conformation of this pentameric structure was almost the same, with root mean-square deviations (rmsd) of less than 0.1 nm, as that in a $T=7$ particle.

Further, in the final stage of fitting, the position of the pentamer was optimized by the reciprocal-space rigid-body refinement between the cryo-EM map and the models. The amino acid residues 297 to 330 connecting the neighboring pentamers were omitted in this procedure. The cryo-EM map was moved into a big P1 cell (cell dimension $a = b = c = 1,000$ Å, $\alpha = \beta = \gamma = 90°$) using the RAVE package of the Uppsala Software Factory (18) to calculate the correlation coefficient at finer grids (24). With the pentamer fivefold axis kept aligned with the icosahedral fivefold axis, the VP1 pentamer was translated along the direction of fivefold axis in 0.1 nm steps from −1.0 to +1.0 nm of the initial position, while at each step it was rotated around the fivefold axis in 1-degree intervals, from 0 to 71 degrees, relative to initial position. During the rigid-body refinement, the

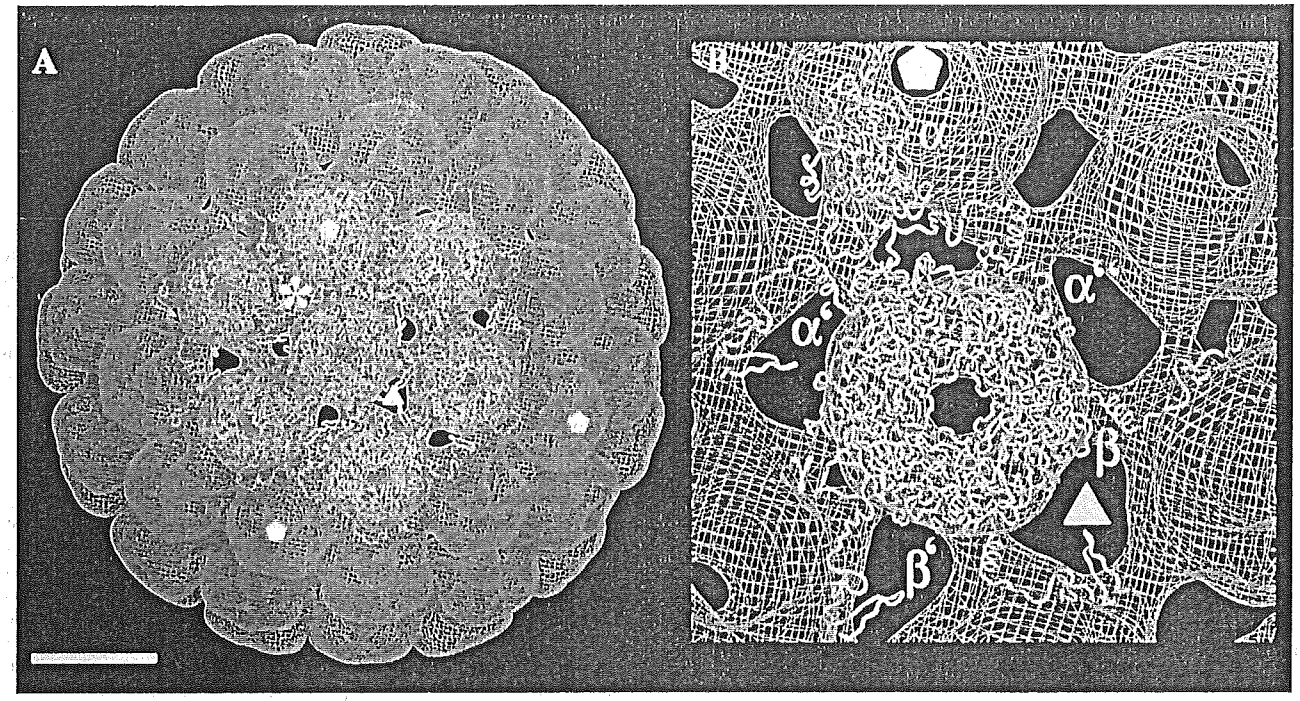

FIG. 5. Fitting of the VP1 model to the density map of the larger $T=7$ particle structure. (A) The density map is viewed along the local sixfold axis, showing the VP1 model fitted to one fivefold pentamer and six local sixfold pentamers. Asterisk, the local threefold position. Bar, 10 nm. (B) Close-up view of the six unique monomers (α, α', and α" at the local threefold; β, β' around the icosahedral threefold; and γ at the twofold). The positions of the threefold and fivefold axes are marked as triangle and pentagons, respectively.

structure of residues 331 to 362 was moved together with the neighboring pentamer. Subsequently, the entire VP1 capsid shell was constructed at each position and orientation according to the icosahedral symmetry. The structure factors were calculated from the models with the B-factor of 100 nm^2 to simulate the resolution limit of the cryo-EM reconstruction map (8, 27), and the correlation coefficient was calculated between the atomic models and the cryo-EM map using CCP4 suite (CCP4, 1994). The pentamer was moved to the position where a maximum correlation coefficient of 0.82 was reached. After the structure that connected the neighboring pentamer was refined, the correlation between the cryo-EM map described above and the final model reached a coefficient of 0.84.

RESULTS

Effect of buffer composition on VLP disassembly and the structure of reassembled particles. The major factors that contributed to the disassembly of $T=7$ VLPs into pentameric capsomers were found to include reduction of disulfide bonds and removal of calcium ions. A combination of a reducing agent and a calcium chelator was required to disassemble the particles. However, dissociation did not occur at very high ionic strength, as seen in the sample treated at ~0.6 M NaCl, in spite of the presence of both reducing agent and EDTA (Fig. 1).

The effect of buffer composition on particle formation from free pentamers was analyzed by dialysis experiments. Samples of free capsomers were exposed to buffers containing different concentrations of $CaCl_2$ and NaCl at various pHs (Fig. 2). Large quantities of small VLPs were formed at low calcium ion concentrations (5 to 10 mM) and in calcium-free buffers. The number of small VLPs decreased when the calcium ion concentration was increased (25 to 100 mM). Although calcium ions were needed to form the $T=7$ VLPs, the number of $T=7$ particles did not change significantly when the calcium ion concentration was increased in the 25 to 100 mM range. At above 300 mM Ca^{2+}, VLP formation was not seen. The concentration of monovalent salt, the pH, or the ionic strength did not directly influence the reassembly of pentamers into higher oligomeric forms.

As mentioned above, a reducing agent was needed to disassemble the BKV VLPs, expressed in insect cells. However, the presence of 2-ME in the reassembly buffer did not prevent the formation of either small or large particles (data not shown).

Three-dimensional reconstruction of the small reassembled BKV VLP. Two BKV VLPs that differed in diameter (26.4 and 50.6 nm) were observed in the low-dose micrograph (Fig. 3). The larger VLPs, with the size of the native virus, were used as an internal reference standard and showed nearly circular image profiles. That indicated that the features of the larger VLPs were well preserved in the vitrified ice. The image profile of the smaller VLPs was also circular, but they did not have the smooth surface of the larger VLPs. Before freezing, the VLP concentration was adjusted so that about 400 particles per micrograph could be selected at the magnification of 45,000.

The structure of the BKV VLP was solved at ~2.4 nm resolution from unstained, frozen-hydrated samples that were imaged with low-irradiation cryo-EM procedures. The three-dimensional reconstruction showed 12 pentameric capsomers in the smaller BKV VLP arranged according to a $T=1$ surface lattice placed on the 12 fivefold rotation axes of the icosahedron (Fig. 4). Due to the smaller diameter of the $T=1$ structure, the unique angle between the capsomers in this particle was 38° greater than that of the average angle between capsomers in the $T=7$ structure (21).

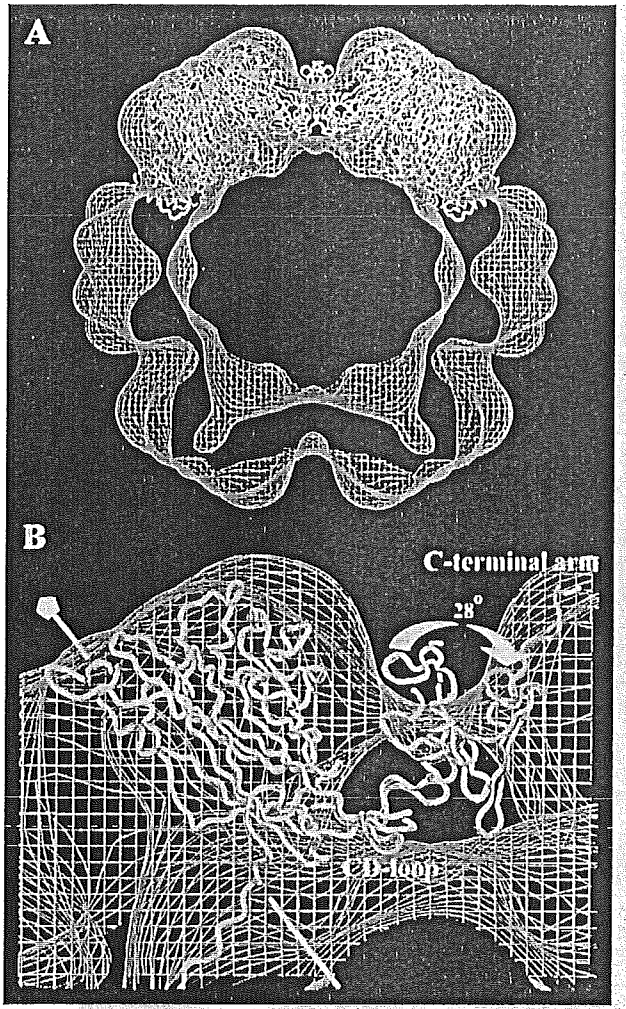

FIG. 6. Fitting of the VP1 model to the density map of the $T=1$ structure. (A) The fivefold monomers from the larger $T=7$ particle were fitted into the density map of the $T=1$ particle. The core of the VP1 model fitted well, while the C-terminal arm was protruding out from the density map at the threefold. This was because the angle between capsomers in the $T=1$ structure was 38 degrees larger than the averaged angle between capsomers in the $T=7$ particle. (B) Parts of two pentamers are seen from the side. There were no structural changes made in the core of the VP1 protein, except for the CD-loop. The unchanged VP1 model is shown in yellow, whereas the modulations made to fit the $T=1$ structure is shown in red. The fivefold axis is marked with a pentagon.

The morphology of the pentameric capsomers was more pronounced in the $T=1$ than in the $T=7$ structure. The $T=1$ capsomers had a diameter of 9.2 nm, which was slightly larger than capsomers in the $T=7$ structure (~1.2 nm larger in diameter). This extra density, compared to the $T=7$ capsomers, was located in the outermost part of each monomer. However, the thickness of the capsid shell was similar, approximately 6.0 nm, in both the $T=1$ and $T=7$ structures.

The major intercapsomeric contact was located at the threefold axis, where the structure protruded from the bottom shell region. The interpentameric contact in the $T=1$ and $T=7$ VLPs at the threefold respective local threefold formed a Y-shaped density connecting three capsomers. This contact remained also when the contour value was raised to 2 sigma (see details in Fig. 7) or following a radial cut of the VLPs capsid shell density. The threefold contact started at a radius of 9.6 nm from the particle center and ended 11.4 nm from the particle center (21.0 to 22.4 nm in the $T=7$ VLP). The density in the twofold axes was much weaker than in the threefold axes. Openings in the capsid shell seen at the threefold and around the twofold axes in the $T=7$ structure were absent in the $T=1$ structure.

Fitting the VP1 model into the density maps of $T=1$ and $T=7$ VLPs. The primary sequence of BKV VP1 has a 74% similarity to the SV40 VP1 that has been solved to a 0.31 nm resolution (34). The similarity is even higher in the C-terminal arm (83%), while the main differences are in the loops at the outer surface of the monomer. A structural model of the BKV VP1 was created by aligning the primary sequence of BKV VP1 with the coordinates of VP1 from SV40 (SV40, PDB: 1SVA). The model of the BKV VP1 was first fit to the density map of the $T=7$ particle to reveal the differences and similarities to particles with the same T-number (Fig. 5A). The only modification required to obtain an excellent fit was an adjustment for the slightly larger radius of the BKV VLP (+0.47 nm of the local sixfold pentamer and +0.58 nm of the fivefold pentamer). The six unique C-terminal arms (α, α', and α'' at the local threefold axis; β, β' around the icosahedral threefold axis; and γ at the twofold axis) (34), responsible for the interpentameric contacts, fitted in the EM density map as well (Fig. 5B).

Each of the six unique monomers was tested as a possible model for the VP1 in the $T=1$ structure. Three of the monomers were excluded because they formed the major interpentameric contact at the twofold axis and had little or no contact at the threefold axis (not shown). In contrast, the three monomers making up the local threefold contact in the $T=7$ structure had their major interpentameric contacts at the threefold axis. The fivefold monomer (α) from the $T=7$ structure was selected as the preferable model of the three, and it was modeled in the density map of the $T=1$ structure.

The core of the VP1 protein (residues 16 to 296) was well fitted to the EM density map (correlation coefficient of 0.82) (Fig. 6A). However, the C-terminal arm protruded out from the density map and did not reach the adjacent capsomer, as the surface curvature was higher within the small-size VLPs compared to the large-size VLPs. Therefore, the angle between the core of VP1 and the outer region of the C-terminal arm required a 28° adjustment in order for the arm to reach the adjacent capsomer (Fig. 6B). The two loops (residues 297 to 300 and 314 to 329) that linked the C-terminal helix to the VP1 protein core and the outermost region of the C-terminal arm were used to increase the angle between the protein core and the C-terminal arm. The last β-strand (the J strand) and the following loop could be modeled in good agreement to the SV40 α monomer. There were, however, additional densities at the side of the monomers. As the structure of the C-terminal domain, covering amino acid residues 348 to 362, had not yet been modeled into the $T=1$ particle, this domain was assumed to account for these additional densities (Fig. 6B).

The structure of the CD loop, which consists of amino acid residues 96 to 106, was rebuilt to that of the α' subunit to avoid a collision with the corresponding loop from an adjacent cap-

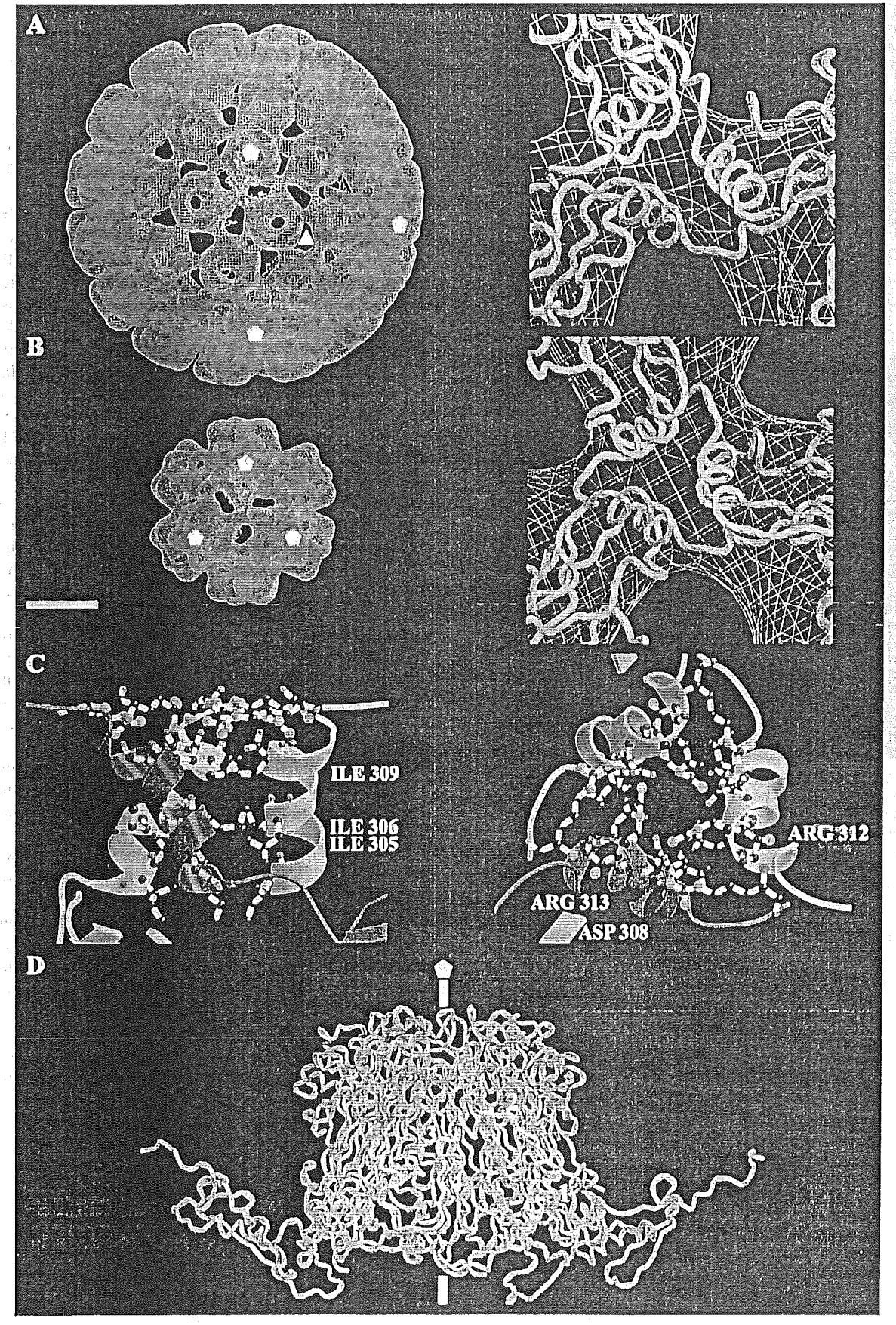
A
B
C
D
ILE 309
ILE 306
ILE 305
ARG 312
ARG 313
ASP 308

somer (34). This region has the highest local root-mean-square deviations between subunits in the $T=7$ particle, suggesting that this region is flexible (Fig. 6B). After refining the C-terminal arm and the CD-loop (the interpentameric connectors), the correlation coefficient between the cryo-EM map, described above, and the final VP1 model reached a value of 0.84.

Interpentameric contacts in the $T=1$ structure. With the adjustments in the C-terminal arm, the structure of a triple-helix bundle, at the threefold axis, was similar to the interpentameric contact at the local threefold axis in the $T=7$ particles (amino acids 300 to 313) (Fig. 7A and B). The three helices were tightly held together by both hydrophobic interactions and salt bridges (Fig. 7C). Furthermore, in the $T=1$ structure the triple-helix bundle was in position to form four hydrogen bonds between each other, which were not seen in the $T=7$ structure. There was, however, a stronger hydrophobic effect within the helix bundle in the $T=7$ structure than in the $T=1$ structure.

To accommodate the higher curvature in the $T=1$ particle than that in the $T=7$ capsid, the C-terminal helix together with the following long loop (amino acids 314 to 329) was tilted 28° away from its own β-barrel core towards the adjacent pentamer. Through this tilt the β-strand J was able to connect with the adjacent pentamer in the $T=1$ structure (Fig. 7D). The long loop, together with the outermost area of the C-terminal arm, composed the region that contributed the least to the interpentameric contact in both the $T=1$ and the $T=7$ capsids. Following the loop, the J-strand made a strong interpentameric contact (with identical interactions as in the $T=7$ structure), starting with one (Glu331) of the two possible calcium-binding amino acids in the C-terminal arm. Amino acid 331 could, however, make an additional salt bridge with amino acid Lys195 in a nearby monomer of the adjacent pentamer. The second amino acid (Asp346) in the C-terminal arm, which was thought to be a calcium-binding site, could establish a salt bridge with amino acid Lys30.

DISCUSSION

The structure of a small VLP of the human BK polyomavirus has been studied and compared with an earlier solved BKV VLP. We have also studied the effect of the buffer composition on VLP disassembly and reassembly processes. The small BKV VLP (26.4 nm in diameter) was shown to have a $T=1$ surface lattice, with a pentamer located at each fivefold axis. In these $T=1$ particles, the main interpentameric contact was found at the icosahedral threefold axis. The angle between the pentamers was 38° greater when compared to the larger BKV VLP (50.6 nm in diameter), which has a capsid composed of 72 pentamers arranged in $T=7$ surface lattices (21). Our observed structure of the $T=1$ particle agrees very well with the computational modeling of the 12-capsomer murine polyomavirus particle done by Salunke et al. (29).

With a 74% similarity to SV40 VP1, the primary sequence of BKV VP1 was aligned with the coordinates of VP1 from SV40 (SV40, PDB:1SVA) to create a structural model of the BKV VP1 (34). This model was first fitted to the density map of the $T=7$ particle in order to reveal the differences and similarities to particles with the same T-number. An excellent fit of the VP1 model to the EM-density map was obtained after an adjustment of the slightly larger diameter of the BKV VLP. The six unique C-terminal arms, responsible for the interpentameric contacts, fitted in the EM density as well.

The fivefold monomer from the $T=7$ structure inserted well into the $T=1$ EM density following an adjustment to particle curvature in the hinge regions of the C-terminal arm. In $T=1$ particles, the pentamers were connected to each other at the icosahedral threefold axis in a similar way as at the local threefold axis in the $T=7$ particle. Here, seen in both particles, the C-terminal arms met in a triple-helix bundle (residues 301 to 313). In the $T=1$ particles this bundle appears to have four additional hydrogen bonds and to be less hydrophobic compared to the $T=7$ structure.

While the outermost part of the C-terminal arm (amino acids 350 to 362) appear to be the most flexible part that do not significantly contribute to the stability of either the small or large VLP, the interactions involving the J-strand is conserved. Thus, the key feature of the capsomer-intervening C-terminal arm is the ability to adjust to the pentamer's relative orientation and particle curvature. In the $T=1$ particle the essential adopting regions are the hinges on both side of the short C-terminal helix. The flexibility in these regions allows the J-strand to insert in the conserved orientation and the short helices from three capsomers to form a bundle, fitting with the cryo-EM map.

A similar type of flexible adaptation in the C-terminal arms has been reported for the $T=1$ and $T=7$ VLPs of the papilloma virus (7, 23). Despite lacking significant sequence similarity, the BKV VP1 (362 residues) and the human papilloma virus 16 L1 (531 residues) both form pentameric capsomers and similar architectures. Also, in the papilloma virus $T=7$ structure the C-terminal arm "invades" adjacent pentamers, keeping the shell together. However, in the $T=1$ structure the C-terminal arms exit the monomer to form the interpentameric contact at the threefold axis and then reinsert into the same monomer.

FIG. 7. Interpentameric interactions in the $T=1$ and $T=7$ BKV VLP. (A) Left: VP1 model of the α (yellow), α′ (red), and α″ (green) monomer fitted to the density map of the $T=7$ particle at the local threefold. Right: close-up of the interpentameric contact "triple-helix bundle" at the local threefold. (B) Left: three $T=1$ VP1 models fitted to the density map of the $T=1$ particle, the particle is viewed along the threefold axis. Right: close-up of the interpentameric contact found at the threefold axis in the $T=1$ particle. (C) Close-up of the triple-helix bundle in the smaller $T=1$ particle, showing possible salt-bridges and hydrophobic interactions. Right, side view; left, top view. (D) The C-terminal arm from the $T=1$ particle (red) and the α monomer from the $T=7$ particle (yellow) are here superimposed to compare interpentameric interactions. The C-terminal arms interact with two monomers in the neighboring pentamer (blue). The C-terminal arms start with a helix at the threefold (in the $T=1$ particle) and at the local threefold in the $T=7$ particle (1). The helix is connected through a long loop (2) to the J-strand (4). The two possible calcium-binding amino acids in the C-terminal arm are also marked, Glu331 (3) and Asp346 (5). The threefold and fivefold are marked as triangle and pentagons, respectively. Bar, 10 nm.

making an elbow-like interpentameric contact. The glycine- and proline-rich sequence, which allows the elbow-like connection in papilloma virus, is not found in the BKV VP1 protein, nor is a similar contact fitting with the structural data available for the BKV VLPs. As a common feature, the variability in the geometry of the contacts in both the polyoma and papilloma virus is entirely due to the inherent flexibility of the C-terminal domains, while the structure of the monomer core (the pentameric ring) seems rather stable and does not change significantly between the $T=1$ and $T=7$ structures. Differing from the papilloma virus case, the $T=1$ and $T=7$ structures of the polyomavirus seem to have one interpentameric interaction in common.

We can here conclude that both Ca^{2+} and disulfide links are important for the stability of the recombinant BKV $T=7$ capsid. However, when the ionic strength of the buffer solution is increased, hydrophobic effects are more influential and keep the capsid intact also in a reducing environment, lacking calcium ions. Chen et al. (6) showed that the reducing and chelating agents worked in a specific order. The reducing agent had to be introduced in advance of the chelating agent in order for dissociation of the VLPs to occur. Thus, the disulfide bond appear to protect bound calcium ions from contact with the chelating agent. Our reassembly experiments also showed that the formation of small or large VLPs does not require the formation of disulfide bonds in vitro. This may suggest that the disulfide interaction is not necessary for the actual reassembly process but that the bond is formed after the particle has been reassembled, allowing for an increase in the stability of the VLP.

Recently, a similar study was done with SV40 VP1, where free pentamers were found to reassemble preferably into the $T=1$ particle in the absence of calcium (17). Contrary to our observations and to those of Salunke et al. (29), Kanesashi et al. (17) did not observe any reassembly into VLPs with buffers having physiological pH (pH 7.2) and salt concentrations (150 mM NaCl). This could be due to the use of a low, 60-μg/ml, protein concentration, compared to the 0.5- to 1-mg/ml concentration used in our and Salunke's experiments.

Both Kanesashi's and our study show that small $T=1$ polyoma VLPs can form without calcium, while the larger $T=7$ structure requires the calcium ion for assembly. Two calcium-binding sites were found in five of the six unique monomers (α, α′, α″, β, and β′), while only one was found in the twofold monomer (γ) in the SV40 structure (34). One amino acid in the C-terminal arm was thought to be involved in each calcium-binding site. Even though the structure in the C-terminal arm was different among the six unique monomers, the interpentameric interactions were quite similar. The difference in structure allowed the same amino acids within the six unique monomers to have similar interpentameric interactions (hydrogen bonds, hydrophobic interactions, or salt bridges) at the three unique interpentameric contacts: at the local threefold axis, around the icosahedral threefold axis, and at the icosahedral twofold axis. However, only in the interpentameric connections at the local threefold and at the icosahedral twofold could the possible calcium-binding amino acids in the C-terminal arm form salt bridges with the adjacent pentamer. The negatively charged amino acids holding the calcium ion would repel each other in its absence. A partial explanation as to why the $T=1$ structure could form without calcium, whereas the $T=7$ structure could not, would then be that only the interpentameric contacts around the $T=7$, icosahedral threefold axis requires calcium for stabilization.

In conclusion, our structural study of the two BKV VLPs has shown that the triple-helix bundle is preserved in both structures and can form without Ca^{2+}. The "flatter" contacts around the threefold axis in the $T=7$ particle is probably both stabilized and enforced by Ca^{2+}, since salt bridges would not substitute in a similar conformation. The calcium concentration will in this way be the critical factor controlling the assembly of the VLPs into different sizes.

Neither of the two assembly models discussed in the literature, namely the assembly nucleus of a "five-around-one" pentamer (34) or a dimer of pentamers (4), can be deduced in our case. All the three unique contacts identified in the BKV VLPs elaborate on the formation of the J strand in the invaded pentamer. As a strong interaction, considerable energy would be needed to replace any type of unique contacts with one another. The primary contact between soluble pentamers would rely on the formation of looser contacts. These are most likely provided by the C-terminal arm at a location before the strand J forming sequence. While further investigations are needed to reveal the steps in which the polyoma VP1 pentamer assembles into particles and virions, our recent data suggests that the position of the C-terminal helix and its following tail could be stabilized through interaction with internal DNA, resulting in a more stable native-like capsid (Nilsson et al., manuscript in preparation).

ACKNOWLEDGMENTS

We thank A. Gutierrez-Rodriguez for his fruitful discussions about protein modeling.

T. Miyamura was supported in parts by grants from the Second Term Comprehensive 10-year Strategy for Cancer Control and by the Program for Promotion of Fundamental Studies in Health Sciences of the Organization for Drug ADR Relief, R&D Promotion and Product Review of Japan (1D:01-3). R. H. Cheng was supported in parts by grants from the Swedish Research council, STINT Foundation, Tripep AB, and Foundation for Knowledge and Competence Development.

REFERENCES

1. Baker, T. S., J. Drak, and M. Bina. 1989. The capsid of small papova viruses contains 72 pentameric capsomers: direct evidence from cryo-EM of simian virus 40. Biophys. J. 55:243–253.
2. Baker, T. S., and R. H. Cheng. 1996. A model-based approach for determining orientations of biological macromolecules imaged by cryoelectron microscopy. J. Struct. Biol. 116:120–130.
3. Brady, J. N., V. D. Winston, and R. A. Consigli. 1977. Dissociation of polyomavirus by the chelation of calcium ions found associated with purified virions. J. Virol. 23:717–724.
4. Casini, G. L., D. Graham, D. Heine, R. L. Garcea, and D. T. Wu. 2004. In vitro papillomavirus capsid assembly analyzed by light scattering. Virology 325:320–327.
5. Chang, D., C. Y. Fung, W. C. Ou, P. C. Chao, S. Y. Li, M. Wang, Y. L. Huang, T. Y. Tzeng, and R. T. Tsai. 1997. Self-assembly of the JC virus major capsid protein, VP1, expressed in insect cells. J. Gen. Virol. 78:1435–1439.
6. Chen, P. L., M. Wang, W. C. Ou, C. K. Lii, L. S. Chen, and D. Chang. 2001. Disulfide bonds stabilize JC virus capsid-like structure by protecting calcium ions from chelation. FEBS Lett. 500:109–113.
7. Chen, X. S., R. L. Garcea, I. Goldberg, G. Casini, and S. C. Harrison. 2000. Structure of small virus-like particles assembled from the L1 protein of human papillomavirus 16. Mol. Cell 5:557–567.
8. Cheng, R. H., V. S. Reddy, N. H. Olson, A. J. Fisher, T. S. Baker, and J. E. Johnson. 1994. Functional implications of quasi-equivalence in a $T=3$ icosahedral animal virus established by cryo-electron microscopy and X-ray crystallography. Structure 2:271–282.
9. Frisque, R. J., G. L. Bream, and M. T. Cannella. 1984. Human polyomavirus JC virus genome. J. Virol. 51:458–469.

10. Fuller, S. D., S. J. Butcher, R. H. Cheng, and T. S. Baker. 1996. Three-dimensional reconstruction of icosahedral particles–the uncommon line. J. Struct. Biol. 116:48–55.
11. Gharakhanian, E., A. K. Sajo, and M. K. Weidman. 1995. SV40 VP1 assembles into disulfide-linked postpentameric complexes in cell-free lysates. Virology 207:251–254.
12. Griffith, J. P., D. L. Griffith, I. Rayment, W. T. Murakami, and D. L. D. Caspar. 1992. Inside polyomavirus at 25-Å resolution. Nature 355:652–654.
13. Haynes, L. L., J. J. Chang, and R. A. Consigli. 1993. Mutations in the putative calcium-binding domain of polyomavirus VP1 affect capsid assembly. J. Virol. 67:2486–2495.
14. Ishizu, K. I., H. Watanabe, S. I. Han, S. N. Kanesashi, M. Hoque, H. Yajima, K. Kataoka, and H. Hand. 2001. Roles of disulfide linkage and calcium ion-mediated interactions in assembly and disassembly of virus-like particles composed of simian virus 40 VP1 capsid protein. J. Virol. 75:61–72.
15. Jao, C. C., M. K. Weidman, A. R. Perez, and E. Gharakhanian. 1999. Cys9, Cys104 and Cys207 of simian virus 40 VP1 are essential for inter-pentamer disulfide-linkage and stabilization in cell-free lysates. J. Gen. Virol. 80:2481–2489.
16. Jones, T. A., J. Y. Zou, S. W. Cowan, and M. Kjeldgaard. 1991. Improved methods for building protein models in electron density maps and the location of errors in these models. Acta Crystallogr. A 47:110–119.
17. Kanesashi, S. N., K. I. Ishizu, M. A. Kawano, S. I. Han, S. Tomita, H. Watanabe, K. Kataoka, and H. Handa. 2003. Simian virus 40 VP1 capsid protein forms polymorphic assemblies in vitro. J. Gen. Virol. 84:1899–1905.
18. Kleywegt, G. J., J. Y. Zou, M. Kjeldgaard, and T. A. Jones. 2001. Around O. *In* M. G. Rossmann and E. Arnold (ed.), International tables for crystallography, vol. F. Crystallography of biological macromolecules, p. 353–356. Kluwer Academic Publishers, Dordrecht, The Netherlands.
19. Li, P. P., A. Nakanishi, S. W. Clark, and H. Kasamatsu. 2002. Formation of transitory intrachain and interchain disulfide bonds accompanies the folding and oligomerization of simian virus 40 vp1 in the cytoplasm. Proc. Natl. Acad. Sci. USA 99:1353–1358.
20. Li, P. P., A. Nakanishi, M. A. Tran, K. I. Ishizu, M. Kawano, M. Phillips, H. Handa, R. C. Liddington, and H. Kasamatsu. 2003. Importance of VP1 calcium-binding residues in assembly, cell entry, and nuclear entry of SV40. J. Virol. 77:7527–7538.
21. Li, T. C., N. Takeda, K. Kato, J. Nilsson, L. Xing, L. Haag, R. H. Cheng, and T. Miyamura. 2003. Characterization of self-assembled virus-like particles of human polyomavirus BK generated by recombinant baculoviruses. Virology 311:115–124.
22. Liddington, R. C., Y. Yan, J. Moulai, R. Sahli, T. L. Benjamin, and S. C. Harrison. 1991. Structure of simian virus 40 at 3.8-A resolution. Nature 354:278–284.
23. Modis, Y., B. L. Trus, and S. C. Harrison. 2002. Atomic model of the papillomavirus capsid. EMBO J. 21:4754–4762.
24. Navaza, J. 1994. AMoRe: an automated package for molecular replacement. Acta Crystallogr. A 50:157–163.
25. Ou, W. C., L. H. Chen, M. Wang, T. H. Hseu, and D. Chang. 2001. Analysis of minimal sequences on JC virus VP1 required for capsid assembly. J. Neurol. Virol. 7:298–301.
26. Rodgers, R. E. D., D. Chang, X. Cai, and R. A. Consigli. 1994. Purification of recombinant budgerigar fledgling disease virus VP1 capsid protein and its ability for in vitro capsid assembly. J. Virol. 68:3386–3390.
27. Rossmann, M. G. 2000. Fitting atomic models into electron-microscopy maps. Acta Crystallogr. D 56:1341–1349.
28. Salunke, D. M., D. L. Caspar, and R. L. Garcea. 1986. Self-assembly of purified polyomavirus capsid protein VP1. Cell 46:895–904.
29. Salunke, D. M., D. L. D. Caspar, and R. L. Garcea. 1989. Polymorphism in the assembly of polyomavirus capsid protein VP1. Biophys. J. 56:887–900.
30. Schmidt, U., R. Rudolph, and G. Böhm. 2000. Mechanism of assembly of recombinant murine polyomavirus-like particles. J. Virol. 74:1658–1662.
31. Schwede, T., J. Kopp, N. Guex, and M. C. Peitsch. 2003. SWISS-MODEL: and automated protein homology-modeling server. Nucleic Acids Res. 31: 3381–3385.
32. Sedzik, J. 1994. DESIGN –A guide to protein crystallization experiments. Arch. Biochem. Biophys. 308:342–348.
33. Stehle, T., Y. Yan, T. L. Benjamin, and S. C. Harrison. 1994. Structure of murine polyomavirus complexed with an oligosaccharide receptor fragment. Nature 369:160–163.
34. Stehle, T., S. J. Gamblin, Y. Yan, and S. C. Harrison. 1996. The structure of simian virus 40 refined at 3.1 Å resolution. Structure 4:165–182.
35. Walker, D. L., and R. J. Frisque. 1986. The biology and molecular biology of JC virus. p. 161–193. *In* N. P. Salzman (ed.) The papovaviridae, vol. 1. Plenum Press, New York, N.Y.
36. Walter, G., and W. Deppert. 1975. Intermolecular disulfide bonds: an important structural feature of the polyomavirus capsid. Cold Spring Harbor Symp. Quant. Biol. 39:255–257.
37. Wickham, T. J., and G. R. Nemerow. 1993. Optimization of growth methods and recombinant protein production in BTI-Tn-5B1-4 insect cells using the baculovirus expression system. Biotechnol. Prog. 9:25–30.
38. Xing, L., K. Kato, T. Li, N. Takeda, T. Miyamura, L. Hammar, and R. H. Cheng. 1999. Recombinant hepatitis E capsid protein self-assembles into dual-domain T=1 particle presenting native virus epitopes. Virology 265:35–45.
39. Xing, L., K. Tjärnlund, B. Lindqvist, G. G. Kaplan, D. Feigelstock, R. H. Cheng, and J. Casanovas. 2000. Distinct cellular receptor interactions in poliovirus and rhinoviruses. EMBO J. 19:5081–5091.
40. Yan, Y., T. Stehle, R. C. Liddington, H. Zhao, and S. C. Harrison. 1996. Structure determination of simian virus 40 and murine polyomavirus by a combination of 30-fold and 5-fold electron-density averaging. Structure 4:157–164.

Journal of Gastroenterology and Hepatology (2005) 20, 1087–1093 DOI: 10.1111/j.1400-1746.2005.03883.x

HEPATOLOGY

Outbreak of hepatitis C virus infection in an outpatient clinic

TAKASHI ISHIKAWA,* YASUSHI FUKUSHIMA,* YUJIRO SHIOBARA,† TSUYOSHI KISHIMOTO,‡ SAKIKO TANNO,‡ IKUO SHOJI,§ TETSURO SUZUKI,§ TAMANO MATSUI,¶ YASUSHI SHIMADA,¶ TAKAAKI OHYAMA,¶ RYOZO NAGAI* AND TATSUO MIYAMURA§

**Department of Internal Medicine, University of Tokyo, Tokyo, †Department of Internal Medicine, Fukaya Red Cross Hospital, Fukaya, ‡Saitama Institute of Public Health, Saitama, §Department of Virology II, National Institute of Infectious Diseases, ¶Infectious Disease Surveillance Center, National Institute of Infectious Diseases, Tokyo, Japan*

Abstract

Background: From January through September 2001, seven patients were admitted to Fukaya Red Cross Hospital with typical clinical manifestations of acute hepatitis. Six were outpatients of the clinic, which is located near the hospital. An extensive survey of clinic outpatients conducted by the local health department revealed six more new acute hepatitis cases during this period.

Methods: A case control study was carried out to identify potential risk factors for infection. In total, 1946 outpatients with clinic records were scheduled to undergo hepatitis C virus (HCV)-antibody testing. For the HCV-Ab positive patients, HCV-RNA was subtyped and quantified, and sequences of HCV hypervariable region 1 were determined.

Results: Ultimately, 12 patients with acute hepatitis and two asymptomatic subjects were found to be a part of this outbreak. HCV isolates were divided into three major groups using phylogenetic tree analysis. Only a past history of visiting the clinic was significantly associated with acute hepatitis. The timing of the parenteral medical procedure at the clinic and the onset of acute hepatitis strongly suggested association of the two events.

Conclusions: Our findings suggest that nosocomial HCV infection can occur in an outpatient clinic, even in countries where post-transfusion hepatitis has been almost entirely eliminated.

© 2005 Blackwell Publishing Asia Pty Ltd

Key words: hepatitis C virus, nosocomial infection, outbreak, outpatient clinic.

INTRODUCTION

Hepatitis C virus (HCV) has infected 170 million people worldwide and the number of deaths annually in the USA from HCV-associated liver disease and cancer may have almost overtaken deaths caused by AIDS.[1–3] HCV causes persistent infection in approximately 80% of infected adults. Severe liver disease and hepatocellular carcinoma develop in an estimated 70% of those who cannot eliminate the virus. The development of a blood screening test in 1990 has virtually eliminated the spread of HCV through transfusions in industrial countries. As a result, the Center for Disease Control (CDC) estimates that new USA HCV infections dropped from approximately 230 000 a year in the 1980s to fewer than 36 000 in 1996. However, the CDC estimates that 1.8% of the USA population still harbors the virus. In Japan, after the introduction of second-generation HCV-Ab tests (February 1992), the risk of post-transfusion HCV infection became essentially negligible.[4,5] The incidence of HCV infection in Japan has decreased to 1.8–3.5/100 000 person-years,[6] which is comparable to that of the USA.[7] Furthermore, in 2000, nationwide nucleic acid amplification testing (NAT) for hepatitis B virus (HBV), HCV and human immunodeficiency virus type 1 (HIV-1) was implemented by the Japanese Red

Correspondence: Takashi Ishikawa, Department of Internal Medicine, University of Tokyo, 7-3-1, Hongo, Bunkyo-ku, Tokyo 113-8655, Japan. Email: takduck-tky@umin.ac.jp

Accepted for publication 31 August 2004.

Cross Blood Transfusion Services for screening of voluntarily donated blood, such that post-transfusion hepatitis C is now virtually nearly zero in Japan.[8]

Nonetheless, nosocomial HCV infections can occur rarely. One way of contracting HCV may be transmission from infected medical personnel to susceptible patients during medical care. Spread from a cardiothoracic surgeon[9] and from an anesthesiology assistant to patients has been reported.[10] Patient-to-patient transmissions were reported in a hematology ward,[11] a pediatric oncology ward,[12] during colonoscopy in a gastrointestinal disease unit,[13] and in a hemodialysis unit.[14,15] Recently, an outbreak of acute hepatitis C among healthy volunteers participating in pharmacokinetics studies was reported.[16] However, nosocomial HCV infection in an outpatient clinic, which is rarely reported for HIV infection,[17,18] has been regarded as extremely rare in industrial countries.

We report here an outbreak of HCV infection at an outpatient clinic in a suburban city near Tokyo, Japan.

METHODS

Description of outbreak

From April through September 2001, seven patients were admitted to Fukaya Red Cross Hospital with typical clinical manifestations of acute hepatitis, including general malaise. HCV antibodies were detected in all seven patients. All seven were infected with HCV genotype 1b. Three patients (F1, F2, F4) were referred by an outpatient clinic (clinic A) located near Fukaya Red Cross Hospital. Three other patients (F3, F5, and F6) with acute hepatitis were from other clinics, but interviews with these patients revealed that they were outpatients of clinic A (Table 1). Only one patient was not an outpatient of clinic A (the serum level of HCV-RNA was negative in this patient when the survey was carried out in May 2001). Sequencing analysis of the serum (convalescent sera stored in November 2001) from the three patients (F 2, F3, F6) revealed sequence similarities among these three patients, which lead the local health department to survey the outpatients of clinic A.

Identification and clinical description of cases

For surveillance purposes, patients were defined as any outpatients who had visited clinic A between July 2000 and May 2002 with symptoms suggestive of acute hepatitis and with serum aspartate aminotransferase (AST) or alanine aminotransferase (ALT) elevation (more than 400 IU/L).

In May 2002, 1946 individuals had outpatient records at clinic A. All 1946 subjects were requested to be tested for HCV-antibody (HCV-Ab). For the HCV-Ab positive patients, confirmation was made by immunoblot assay (RIBA; recombinant immunoblot assay: Ortho-Clinical-Diagnostics, Raritan, NJ, USA), HCV-RNAs were subtyped, and quantified.

Laboratory methods

Serum samples from the patients were collected in May 2002 and frozen at −80°C. The presence of HCV-Ab was determined by the gelatin particle agglutination test (Ortho-Clinical-Diagnostics). Reactivity was confirmed by immunoblot assay (RIBA). HCV RNA was detected qualitatively and was also quantified with reverse transcription-polymerase chain reaction (RT-PCR) kits (HCV Amplicore v2.0; Roche Diagnostics, Tokyo, Japan). HCV isolates were genotyped, and HCV hypervariable region 1 (HVR1: nucleotides 1491–1572, numbered as reported by Choo *et al.*[19]) was amplified as described elsewhere.[20] Products of the second PCR were purified from the agarose gel and cloned into a plasmid vector (TOPO TA cloning kit; Invitrogen, Carlsbad, CA, USA). Four to six clones from each subject were sequenced in both directions with CEQ2000 (Beckman Coulter, Fullerton, CA, USA). The direct

Table 1 Clinical characteristics of patients with acute hepatitis C

Case	Sex	Age	ALT (IU/L)	Peak T Bil (mg/dL)	Peak	Onset genotype
F1	Female	71	991	1.9	January 2001	1b
F2	Female	68	3645	14.1	April 2001	1b
F3	Female	24	2365	7.0	April 2001	1b
F4	Female	54	918	1.9	April 2001	1b
F5	Male	26	1077	1.7	July 2001	1b
F6	Male	76	1590	11.2	September 2001	1b
N1	Female	40	554	0.8	December 2000	1b
N2	Female	83	1950	15.9	April 2001	1b
N3	Male	73	1370	9.6	May 2001	1b
N4	Male	77	421	1.0	June 2001	1b
N5	Female	71	800	3.0	August 2001	1b
N6	Male	61	594	0.9	August 2001	1b

ALT, alanine aminotransferase; T Bil, total bilirubin.

sequencing procedures were performed with the primers used in the second PCRs employing a Dye Terminator Cycle Sequencing Kit (Perkin Elmer, NJ, USA) and analyzed on an ABI PRISM 377 sequencer. To prevent possible cross-contamination of the samples, stringent procedures were used for nucleic acid extraction and amplification, and the analyses were performed independently in two laboratories (Tokyo University and National Institute of Infectious Diseases) separately. Identical sequence results were obtained.

Pylogenetic analysis

The degree of divergence between the sequences was estimated by the neighbor-joining (NJ) method using Kimura's two-parameter distance.[21] The set of distance matrices was then analyzed by the UPGMA (Unweighted Pair Group Method with Arithmetic Mean) program of the Genetyx-Mac (version 10.1., Software Development, Tokyo, Japan).

Case control study and statistical analysis

We conducted two case control studies. In the first case control study, we enrolled seven patients and 11 matched controls from among the outpatients of Fukaya Red Cross Hospital to identify potential risk factors for infection. We used a detailed questionnaire to interview patients and controls. Information included past history of blood transfusion, surgical operation, tattooing, drug abuse, familial liver diseases, and parenteral procedures at clinic A. Parenteral procedures were confirmed by the records of patients at clinic A.

In the second case control study, we enrolled the first nine (F1-F6, N2-N4) patients and matched 18 controls from among outpatients of clinic A to identify potential risk factors for HCV outbreak. We used a detailed questionnaire to interview patients and controls. Collected information included past history of blood transfusion, surgical operation, tattooing, drug abuse, familial liver diseases, and parenteral treatment at clinic A. The parenteral treatments included blood aspiration, percutaneous injection, intravenous pyelography, intravenous cholangiography, endoscopy, intravenous injection, and drip infusion.

In the case control study, odds ratios and 95% confidence intervals were calculated with the use of Statview Version 5.0 (SAS Institute, Cary, NC, USA).

RESULTS

Survey of outpatients

An active survey revealed six more patients (N1-N6) with acute hepatitis C among outpatients of clinic A (Table 1). Three (N2, N3, N4) had received injection therapy and had been followed up in the clinic. The other three (N1, N5, N6) patients had visited other clinics with typical manifestations of acute hepatitis. A nurse (N1) who had worked at clinic A (through December 2000) had been diagnosed with acute hepatitis in December 2000. Thus, the total number of patients with acute hepatitis C virus infection in this outbreak was 12 (Fig. 1). The clinical characteristics of these patients are summarized in Table 1.

To define the extent of the outbreak, we notified all patients who had visited clinic A and had received any form of parenteral therapy from July 2001 through to May 2002. Those patients were contacted by local health department personnel, and a brief, standardized questionnaire was administered.

Altogether, 1831 patients (94.1%) out of 1946 with outpatient records of clinic A were surveyed from May through December 2002. In total, 1776 of the 1831 tested patients had age data, while for the other 51 patients no age data were available. Those 51 outpatients were HCV-Ab negative. Age related HCV-Ab positivity was as follows: 0–9 years old; 0/197, 10–19 years old; 0/294, 20–29 years old; 0/228, 30–39 years old; 1/187, 40–49 years old; 8/203, 50–59 years old; 2/298, 60–69 years old; 10/209, 70–79 years old; 12/122, and over 80 years old; 3/42. Thirty-six (including six new cases: N1-N6 with acute hepatitis) patients (2.0%) were HCV-Ab positive. Of these 36 HCV-Ab positive patients, 20 had genotype 1b, six had genotype 2a, two had genotype 2b, and eight had the virus undetectable according to the HCV quantification analysis.

In May 2002, the HCV-RNA level remained high in all 12 patients with acute hepatitis and ALT was slightly elevated. None of these patients in this outbreak had cleared the virus in at least 10 months after the infection. All staff members (two doctors and three nurses), except the nurse (N1) who had acute hepatitis, were negative for HCV-Ab on third-generation assays.

Molecular comparison

The HCV isolates of the 12 patients (F1-F6, N1-N6) with acute hepatitis and the 14 (out of 20 excluding six new patients with acute hepatitis) HCV-RNA positive carriers with genotype 1b were determined by HVR1

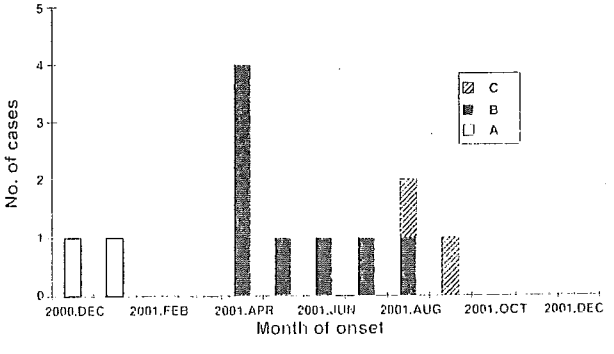

Figure 1 Onsets of hepatitis C virus (HCV) infection during the outbreak, according to the date of diagnosis. a-c shows the three major groups of HCV isolates in the outbreak that is described in Figure 2.

sequences. The HCV isolates of the patients with acute hepatitis were divided into three groups. The HVR1 sequences of two patients (AS1 and AS2) of the 14 asymptomatic patients were similar to those of patients with acute hepatitis, while those of the other 12 were not. Figure 2a shows the amino acid sequences of HVR1 for each of the isolates. The evolutionary distances in this outbreak were similar to those previously reported for HCV infections caused by needle-stick injuries.[22] HCV isolates were divided into three major groups using phylogenetic tree analysis. The first group (group A) consists of two patients, F1 and N1. HCV isolates from these two patients diverged from other isolates, but F1 and N1 had amino acid mutations in common.

The second group (group B) represented the major HCV type in this outbreak. F2 and F4 showed identical isolates and phylogenetic tree analysis strongly suggested that these patients were infected with the same HCV (Fig. 2b). Two asymptomatic carriers (AS1 and AS2) belonged to this group. It is difficult to determine whether these two patients were infected in this outbreak or were possible sources of this HCV infection. The third group (group C) consists of F6 and N5, who had completely identical sequences. These isolates diverged from group A, but had common amino acid substitutions with those of group B.

a

```
Group A
N1:  VLLLFAGVDGSTYTTGAKVGHSTSSFASLFQTGSQQKLQLINTNGSWHIN
F1:  ------------I---N-RG----I-G-R--------------------

Group B
F2:  VMLLFAGVDGQTRVSGGTAGHTARGVASLFSPGASQNIQLINTNGSWHIH
F3:  ------------------------LT----S------------------
F4:  ------------------------------------------------
F5:  ----------H----------A----T--------------------
N2:  ------------------------------F------------------
N3:  ----------G-H-T---T------------S------------------
N4:  ------------------------------------------------
N6:  -----S--------------------T----F------------------
AS1: ------------------------------F------------------
AS2: ------------------------------F------------------
Group C

F6:  --------------T---TS--NTH-LV-------R--------------
N5:  ------------------------------------------------

Controls
B10: --------------T--AS-FNT-TLT---HS-P--K---V-S-------
B13: ----------S---T--NVGRG-SGLSG---Y-SA-K---V---------
B14  ----------N-H-T--AQARATSKF--F-ALGP--K---V---------
```

b

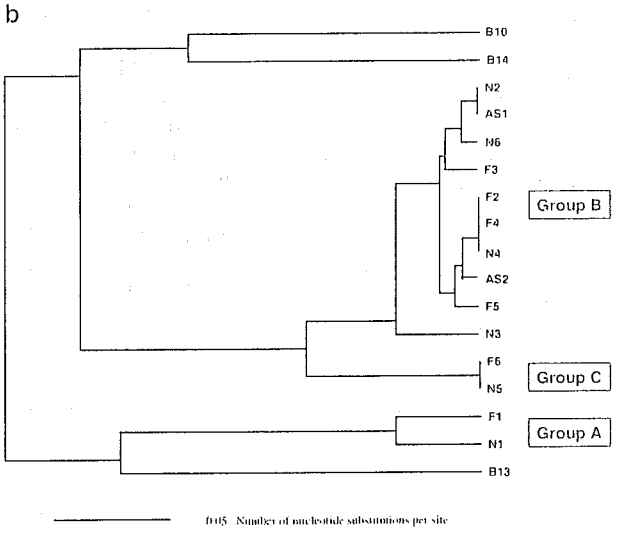

Figure 2 (a) Alignment of the amino acid sequences of hepatitis C virus (HCV) hypervariable region 1 from the patients. HCV isolates were divided into three major groups (groups A, B and C). AS1 and AS 2 are asymptomatic patients. The dashes denote amino acids identical to N1 in group A, and to F2 in group B, C, and control groups. Polymerase chain reaction (PCR) products of HCV isolates obtained from chronic hepatitis C patients in other areas were used as controls. (b) Phylogenetic tree analysis comparing coding sequences for HCV hypervariable region 1 from 17 isolates. For phylogenetic analysis, HVR1 sequences obtained from 14 HCV-RNA positive patients involved in this outbreak and three controls were compared.

Evaluation of risk factors for hepatitis C virus infection

In the first case control study, only a past history of visiting clinic A was significantly associated with acute hepatitis (OR, 42.6; 95% CI, 2.28–177.3). In the second case control study, intravenous pyelography (OR, 2.50; 95% CI, 0.24–25.68), intravenous cholangiography (OR, 2.50; 95% CI, 0.47–13.27), and drip infusion (OR, 2.14; 95% CI, 0.25–18.50) showed relatively high OR, but were not significantly associated with acute hepatitis. It is difficult to identify potential risk factors because controls had also received several parenteral treatments. Almost all patients and controls had undergone at least one of the parenteral procedures at this clinic (Table 2).

To determine the source of outbreak, we reviewed individual patient records. Each patient with acute hepatitis had received at least one of the following parenteral medical procedures; blood aspiration, percutaneous injection, intravenous pyelography, intravenous cholangiography, endoscopy, intravenous injection, or drip infusion. Figure 3 shows the relationship between

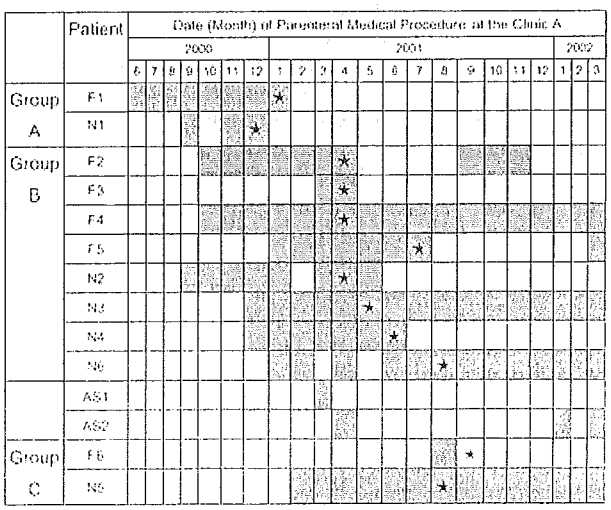

Figure 3 Relationship between a parenteral medical procedure and the onset of acute hepatitis. (★) show the onset of acute hepatitis.

Table 2 Risk factors possibly associated with parenteral medical procedures

Risk factor	Cases +	Cases −	Controls +	Controls −	OR	95% CI
Blood aspiration	9	0	17	1	1.11	0.09–13.84
Percutaneous injection	9	0	17	1	1.11	0.09–13.84
Intravenous pyelography	9	0	15	3	2.50	0.24–25.68
Cholangiography	6	3	8	10	2.50	0.47–13.27
Endoscopy	1	8	2	15	0.94	0.07–12.00
Intravenous injection	0	9	0	17	1.80	0.10–31.99
Drip infusion	2	7	2	15	2.14	0.25–18.50

Intravenous pyelography, intravenous cholangiography, and drip infusion showed relatively high odds ratio (OR). It is difficult to identify potential risk factors because controls had also received several parenteral treatments. CI, confidence interval.

the parenteral procedure and the onset of acute hepatitis. This data strongly suggests an association between the onset of acute hepatitis and parenteral treatment at clinic A. Patient F3 had visited clinic A only once in March 2001, and had received a percutaneous injection and intravenous pyelography, and manifested acute hepatitis in April.

DISCUSSION

We reported an outbreak of HCV infection in an outpatient clinic. Most of the patients had typical manifestations of acute hepatitis. Acute HCV infection is usually asymptomatic, despite significant viremia and hepatic cytolysis. Only one-third of patients develop jaundice or symptoms.[23] One of the characteristics of this outbreak was that most of the patients had accompanying symptoms of general malaise or jaundice. Although all patients recovered, the symptoms in the acute phase were severe and peak ALT levels were relatively high. The serum level of HCV-RNA had persisted in all patients at least 10 months after the infection. Only two asymptomatic carriers were identified in the retrospective survey of outpatients, suggesting that a high percentage of patients were symptomatic in this outbreak. Although drug abuse, high-risk sexual behavior, and poverty are considered to be risk factors for HCV infection,[24] these risk factors were not identified in the present outbreak. No surgical exposure prone procedures were found in this clinic.

Transmission risk is determined by the infectivity of the body fluids and tissues to which an individual is exposed. In this sense, HCV RNA concentrations in the inocula were assumed to be high. Alternatively, the HCV isolates in this outbreak may have been exceptionally infectious. We cannot rule out either of these possibilities.

The mean incubation period to onset of symptoms is about 7 weeks (range: 3–20 weeks)[23] in acute hepatitis C. All patients in this outbreak had at least one parenteral treatment at clinic A 7–8 weeks before the onset of symptoms (Fig. 3), suggesting that the infection was contracted when these procedures were carried out. The survey of the clinic by the local health department showed that glass syringes had been used after sterilization with an autoclave until 2001. Previously, an iatrogenic HCV infection with glass syringes was suggested in parenteral antischistomal therapy in Egypt[25] and in a rural area of Japan.[26] Furthermore, it was found that bottles had been shared among several patients receiving parenteral treatments, particularly percutaneous injection, intravenous pyelography, intravenous cholangiography, and drip infusion. It is probable that the needles were exchanged, but the injection equipment, including the bottles, was used for several patients. This may have been the source of the infection.

Fukaya city is a suburb of Tokyo, with a population of approximately 100 000. The incidence of HCV infection in Japan has fallen to less than 1.8–3.5/100 000 person-years,[6] which is comparable to that of the USA. In Japan and Italy,[27] the proportions of HCV positive patients are higher among the elderly (particularly those in their sixties and older in contrast to the USA where the incidence is highest in the fourth and fifth decades [3.0–3.9%]).[28] We must keep in mind that some percentage of the general population will have HCV infection, and can become a reservoir for an acute HCV outbreak even in general practice. Minor violations in safety procedures may result in the spread of blood borne agents even in the countries where the incidence of HCV infection is low.

Characteristic features of this outbreak are its high percentage of chronicity. None of the patients with acute hepatitis had eliminated HCV before May 2002. Symptomatic acute hepatitis C infection has been described to have a better outcome.[29,30] Lately, in the study of the natural course of acute symptomatic hepatitis C, spontaneous clearance was observed in 52% of the patients, usually within 12 weeks after the onset of symptoms.[31] Treatment of acute hepatitis C with interferon alfa-2b was reported to be very effective, if the patients started to receive interferon within the preceding 4 months after the known or suspected exposure.[32] In this outbreak, at least 10 months had passed after the suspected exposure, so for some of the patients under 60 years of age, we started ribavirin plus interferon therapy.[33] However, for those over 70 we are

conducting periodic follow-up, because in studies with 10–20 years of follow-up, cirrhosis develops in less than 20–30% of patients.[30]

Epidemiological and phylogenetic analyses disclosed horizontal nosocomial HCV infection. We were not able to pinpoint the precise mechanisms leading to these infections. Nonetheless, this study underlies the importance of constant surveillance of infectious diseases. Our findings suggest that nosocomial HCV infection can occur in an outpatient clinic, even in countries where post-transfusion hepatitis is apparently well controlled.

REFERENCES

1 Lauer GM, Walker BD. Hepatitis C virus infection. *N. Engl. J. Med.* 2001; 345: 41–52.
2 Cohen J. The scientific challenge of hepatitis C. *Science* 1999; 285: 26–30.
3 El-Serag HB, Mason AC. Rising incidence of hepatocellular carcinoma in the United States. *N. Engl. J. Med.* 1999; 340: 745–50.
4 Japan Red Cross Non-A, Non-B Hepatitis Reseach Group. Effect of screening for hepatitis C virus antibody and hepatitis B virus core antibody on incidence of post-transfusion hepatitis. *Lancet* 1991; 338: 1040–1.
5 Sasaki F, Tanaka J, Moriya T *et al.* Very low incidence rates of community-acquired hepatitis C virus infection in company employees, long-term inpatients, and blood donors in Japan. *J. Epidemiol.* 1996; 6: 198–203.
6 Yoshizawa H. Hepatocellular carcinoma associated with hepatitis C virus infection in Japan: projection to other countries in the foreseeable future. *Oncology* 2002; 62 (Suppl. 1): 8–17.
7 Schreiber GB, Busch MP, Kleinman SH, Korelitz JJ. The risk of transfusion-transmitted viral infections. The retrovirus epidemiology donor study. *N. Engl. J. Med.* 1996; 334: 1685–90.
8 Ohnuma H, Tanaka T, Yoshikawa A *et al.* The first large-scale nucleic acid amplification testing (NAT) of donated blood using multiplex reagent for simultaneous detection of HBV, HCV, and HIV-1 and significance of NAT for HBV. *Microbiol. Immunol.* 2001; 45: 667–72.
9 Esteban JI, Gomez J, Martell M *et al.* Transmission of hepatitis C virus by a cardiac surgeon. *N. Engl. J. Med.* 1996; 334: 555–60.
10 Ross RS, Viazov S, Gross T, Hofmann F, Seipp HM, Roggendorf M. Transmission of hepatitis C virus from a patient to an anesthesiology assistant to five patients. *N. Engl. J. Med.* 2000; 343: 1851–4.
11 Allander T, Gruber A, Naghavi M *et al.* Frequent patient-to-patient transmission of hepatitis C virus in a haematology ward. *Lancet* 1995; 345: 603–7.
12 Widell A, Christensson B, Wiebe T *et al.* Epidemiologic and molecular investigation of outbreaks of hepatitis C virus infection on a pediatric oncology service. *Ann. Intern. Med.* 1999; 130: 130–4.
13 Bronowicki JP, Venard V, Botte C *et al.* Patient-to-patient transmission of hepatitis C virus during colonoscopy. *N. Engl. J. Med.* 1997; 337: 237–40.
14 Allander T, Medin C, Jacobson SH, Grillner L, Persson MA. Hepatitis C transmission in a hemodialysis unit: molecular evidence for spread of virus among patients not sharing equipment. *J. Med. Virol.* 1994; 43: 415–19.
15 Halfon P, Roubicek C, Gerolami V *et al.* Use of phylogenetic analysis of hepatitis C virus (HCV) hypervariable region 1 sequences to trace an outbreak of HCV in an autodialysis unit. *J. Clin. Microbiol.* 2002; 40: 1541–5.
16 Larghi A, Zuin M, Crosignani A *et al.* Outcome of an outbreak of acute hepatitis C among healthy volunteers participating in pharmacokinetics studies. *Hepatology* 2002; 36: 993–1000.
17 Ou CY, Ciesielski CA, Myers G *et al.* Molecular epidemiology of HIV transmission in a dental practice. *Science* 1992; 256: 1165–71.
18 Katzenstein TL, Jorgensen LB, Permin H *et al.* Nosocomial HIV-transmission in an outpatient clinic detected by epidemiological and phylogenetic analyses. *AIDS* 1999; 13: 1737–44.
19 Choo QL, Kuo G, Weiner AJ, Overby LR, Bradley DW, Houghton M. Isolation of a cDNA clone derived from a blood-borne non-A, non-B viral hepatitis genome. *Science* 1989; 244: 359–62.
20 Okada S, Akahane Y, Suzuki H, Okamoto H, Mishiro S. The degree of variability in the amino terminal region of the E2/NS1 protein of hepatitis C virus correlates with responsiveness to interferon therapy in viremic patients. *Hepatology* 1992; 16: 619–24.
21 Brown A. Methods in evolutionary analysis of viral sequences. In: Morse SSE, ed. *The Evolutionary Biology of Viruses*. New York: Raven Press, 1994; 75–84.
22 Suzuki K, Mizokami M, Lau JY *et al.* Confirmation of hepatitis C virus transmission through needlestick accidents by molecular evolutionary analysis. *J. Infect. Dis.* 1994; 170: 1575–8.
23 Hoofnagle JH. Hepatitis C: the clinical spectrum of disease. *Hepatology* 1997; 26: 15S–20S.
24 Alter MJ. Epidemiology of hepatitis C. *Hepatology* 1997; 26: 62S–65S.
25 Frank C, Mohamed MK, Strickland GT *et al.* The role of parenteral antischistosomal therapy in the spread of hepatitis C virus in Egypt. *Lancet* 2000; 355: 887–91.
26 Hayashi J, Kishihara Y, Yamaji K *et al.* Transmission of hepatitis C virus by health care workers in a rural area of Japan. *Am. J. Gastroenterol.* 1995; 90: 794–9.
27 Guadagnino V, Stroffolini T, Rapicetta M *et al.* Prevalence, risk factors, and genotype distribution of hepatitis C virus infection in the general population: a community-based survey in southern Italy. *Hepatology* 1997; 26: 1006–11.
28 Alter MJ, Kruszon-Moran D, Nainan OV *et al.* The prevalence of hepatitis C virus infection in the United States, 1988 through 1994. *N. Engl. J. Med.* 1999; 341: 556–62.
29 Vogt M, Lang T, Frosner G *et al.* Prevalence and clinical outcome of hepatitis C infection in children who underwent cardiac surgery before the implementation of blood-donor screening. *N. Engl. J. Med.* 1999; 341: 866–70.
30 Kenny-Walsh E. Clinical outcomes after hepatitis C infection from contaminated anti-D immune globulin. Irish Hepatology Research Group. *N. Engl. J. Med.* 1999; 340: 1228–33.
31 Gerlach JT, Diepolder HM, Zachoval R *et al.* Acute hepatitis C: high rate of both spontaneous and treatment-induced viral clearance. *Gastroenterology* 2003; 125: 80–8.

32 Jaeckel E, Cornberg M, Wedemeyer H *et al.* Treatment of acute hepatitis C with interferon alfa-2b. *N. Engl. J. Med.* 2001; 345: 1452–7.
33 McHutchison JG, Gordon SC, Schiff ER *et al.* Interferon alfa-2b alone or in combination with ribavirin as initial treatment for chronic hepatitis C. Hepatitis Interventional Therapy Group. *N. Engl. J. Med.* 1998; 339: 1485–92.

JOURNAL OF CLINICAL MICROBIOLOGY, Sept. 2005, p. 4413–4417 Vol. 43, No. 9
0095-1137/05/$08.00+0 doi:10.1128/JCM.43.9.4413–4417.2005
Copyright © 2005, American Society for Microbiology. All Rights Reserved.

Quantitative Detection of Hepatitis C Virus (HCV) RNA in Saliva and Gingival Crevicular Fluid of HCV-Infected Patients

Tetsuro Suzuki,[1]* Kazuhiko Omata,[1,2] Tazuko Satoh,[2] Takahiro Miyasaka,[2] Chiaki Arai,[3] Munehiro Maeda,[4] Tomonori Matsuno,[2] and Tatsuo Miyamura[1]

Department of Virology II, National Institute of Infectious Diseases,[1] Department of Oral and Maxillofacial Surgery[2] and Department of Endodontics and Operative Dentistry,[4] The Nippon Dental University School of Dentistry at Tokyo, and Section of Clinical Laboratory, The Nippon Dental University School of Dentistry at Tokyo Hospital,[3] Tokyo, Japan

Received 8 February 2005/Returned for modification 28 May 2005/Accepted 2 June 2005

The search for hepatitis C virus (HCV) in body fluids other than blood is important when assessing possible nonparenteral routes of viral transmission. However, the role of oral fluids in HCV transmission remains controversial. Here we quantitatively determined HCV RNA in saliva and gingival crevicular fluid (GCF) of anti-HCV-positive patients. Most patients (14 of 18; 78%) whose saliva specimens were negative had HCV RNA in their GCF. Most patients (20 of 26; 77%) had higher HCV RNA levels in their GCF than in their saliva. Although there was not a statistically significant correlation between the serum viral load and HCV level in saliva or GCF, patients with low serum HCV loads were less likely to have detectable HCV in their saliva. These findings have important implications for medical personnel and suggest that epidemiological studies designed to understand the significance of the oral route of transmission of HCV are warranted.

Hepatitis C virus (HCV) infection represents a major public health problem in the world today. The infection primarily causes liver disease; however, HCV infection has also been associated with extrahepatic abnormalities, including mixed cryoglobulinemia, malignant lymphoma, Sjögren's syndrome, and oral lichen planus (2, 12, 18, 19, 34, 39). Lymphotropism of HCV has been observed, and several laboratories have detected the virus in blood mononuclear cells (BMC) (16, 22, 26, 28, 35, 38). Common risk factors for HCV infection include blood transfusion from unscreened donors as well as injection drug use. Although sexual and vertical transmissions have also been reported, there remain a large number of HCV carriers in whom no route of infection has been identified.

Epidemiological surveys demonstrate that body fluids other than blood, including saliva, might be potential sources of HCV infection. Experimental inoculation of saliva obtained from chronic HCV carrier chimpanzees has been reported to transmit hepatitis to recipient animals (1). Several studies have demonstrated HCV RNA in the saliva of hepatitis C patients by reverse transcription (RT)-nested PCR. However, the detection rates of viral RNA within saliva have varied widely, and some groups have failed to demonstrate HCV RNA within saliva (6–11, 14, 17, 23, 25, 27, 29–33, 36–38). A potential source of HCV RNA within saliva includes gingival crevicular fluid (GCF), which might contain HCV-infected BMC in the setting of periodontal inflammation. To our knowledge, only one study has qualitatively identified HCV in GCF; HCV RNA was detected in 59% of GCF specimens from hepatitis C patients in the study (20). Since the efficiency of HCV transmission is likely related to its viral load, it is important to quantitate viral RNA levels within body fluids in order to properly evaluate possible nonparenteral routes of HCV infection.

Thus, we examined the presence of HCV RNA in the saliva and GCF of anti-HCV antibody-positive patients using real-time quantitative RT-PCR.

MATERIALS AND METHODS

Sample collection. Twenty-six dental patients attending the hospital of Nippon Dental University at Tokyo were studied. All of the patients were anti-HCV antibody seropositive on the basis of screening using a second-generation enzyme immunoassay (Abbott HCV PHA, Abbott Diagnostics, Abbott Park, IL). This study protocol was approved by the Ethics Committee of the hospital and was conducted according to *Ethic Guideline for the Studies on Human Genome and Gene Analysis*. Written informed consent was obtained from each patient participating in the study.

Blood samples were collected and centrifuged for 20 min at 5,000 rpm to separate the serum. Patients spit into a cup to obtain saliva samples. Whole saliva samples (approximately 2 ml) were then transferred into sterile containers. None of the samples were macroscopically observed to contain blood. GCF specimens were collected by first drying the gingival surface with sterile cotton, after which the area was isolated in order to prevent contamination with saliva. A paper strip (2 by 5 mm) was then subgingivally inserted for 30 s to collect specimens (approximately 50 μl). If there was visible contamination of the sample with blood, another sample without macroscopic blood contamination was taken from another site. The depth at gingival crevices was then measured by a periodontal probe, and the presence of bleeding on probing was examined. Serum, saliva, and GCF samples were collected simultaneously and were stored at −80°C before use.

RNA extraction. Total RNA was extracted from 100 μl of serum or saliva specimens and from paper strips with collected GCF using a QIAamp viral RNA kit (QIAGEN, Valencia, CA). In preliminary experiments using various amounts of serum, saliva, and GCF samples in the presence or absence of paper strips, we confirmed that (i) sample volumes of ≥40 μl yielded the same efficiencies of RNA extraction from each specimen and (ii) inclusion of a paper strip described above in the lysis buffer did not influence the efficiency of RNA extraction.

Quantitation of HCV RNA. To determine the quantity of HCV RNA, real-time RT-PCR involving single-tube reactions was performed using TaqMan EZ RT-PCR Core reagents (PE Applied Biosystems, Foster City, CA), as previously described (3). Briefly, the reaction mixture contained 1× TaqMan EZ buffer, 500 nM concentrations of each primer from the HCV 5′ noncoding region (5′-GAG TGT CGT GCA GCC TCC A-3′ and 5′-CAC TCG CAA GCA CCC TAT CA-3′), a 200 nM concentration of fluorogenic probe [5′-(6-carboxyfluorescein)

* Corresponding author. Mailing address: Department of Virology II, National Institute of Infectious Diseases, 2-14-15 Toyama, Shinjuku-ku, Tokyo, Japan 162-8640. Phone: (81) 3-5285-1111. Fax: (81) 3-5285-1161. E-mail: tesuzuki@nih.go.jp.

TABLE 1. Clinical and virological characteristics of 26 patients examined in this study[a]

Age	Gender	ALT level (IU/liter)	AST level (IU/liter)	HCV antibody titer (2[n])	Genotype	Oral disease(s)
68	F	30	48	>12	1b	
64	M	115	103	>12	1b	Periodontitis/BOP
71	F	14	23	12	2b	Periodontitis/BOP
71	M	124	71	12	1b	Periodontitis/BOP
71	M	47	55	12	1b	
63	M	14	19	11	1b	SCC
66	F	59	67	11	1b	OLP
61	F	61	35	11	1b	
73	F	48	40	10	2a	Periodontitis/BOP
70	F	18	25	10	1b	Periodontitis/BOP, OLP
72	F	15	20	8	1b	Periodontitis/BOP
61	M	7	12	8	ND	Periodontitis
66	F	19	30	8	1b	OLP
69	F	31	39	7	ND	SCC
73	M	16	24	6	ND	Periodontitis/BOP, SCC
72	F	20	22	6	ND	
67	M	12	18	4	ND	Periodontitis/BOP, SCC
70	F	5	17	4	ND	Periodontitis/BOP, SCC
69	M	13	20	4	1b	Periodontitis/BOP, SCC
60	M	22	23	4	1b	Periodontitis
71	F	15	30	4	ND	SCC
56	F	11	17	4	ND	Periodontitis/BOP, OLP
71	F	12	21	4	ND	Periodontitis/BOP
67	F	9	24	4	ND	
58	M	26	25	4	ND	
79	F	22	21	4	ND	

[a] Abbreviations: F, female; M, male; ND, not detected; OLP, oral lichen planus; BOP, bleeding on probing; SCC, squamous cell carcinoma.

CCC GCA AGA CTG CTA GCC GAG TAG TGT TGG (6-carboxytetramethylrhodamine)-3′], 200 μM concentrations of each deoxynucleoside triphosphate, 3 mM $Mn(OAc)_2$, 5 U of *Thermus thermophilus* DNA polymerase, 0.5 U of AmpErase uracil *N*-glycosylase, and template RNA. The primers and probe were designed on the basis of the conserved sequences among HCV genotypes. The RT step was started with a 1-min incubation at 50°C, followed by 50 min at 65°C. Thermal cycling conditions were as follows: a precycling period of 5 min at 95°Cfollowed by 50 cycles of denaturation at 94°C for 15 s and annealing at 55°C for 10 s and extension at 69°C for 1 min. All reactions and analyses of the amplification plots were performed on an Applied Biosystems PRISM 7700 sequence detector (PE Applied Biosystems). Standard curves of the assays were obtained by plotting 10-fold serial dilutions of known concentrations of a synthetic HCV genotype 1b transcript. HCV RNA copy numbers of the synthetic transcript were calculated from the quantity and its molecular weight. Using a standard curve, the Sequence Detector software calculated automatically the concentration of RNA copies in the experimental samples. We found that results obtained from our in-house real-time RT-PCR method were well correlated with those from the COBAS AMPLICOR HCV MONITOR Test, version 2.0 (Roche Diagnostics, Tokyo, Japan) (15), and that 1 HCV RNA copy/ml in our method corresponded to approximately 1 international unit/ml by the above-mentioned commercial assay (data not shown).

HCV genotyping. HCV genotype was determined by RT-PCR of the core region sequence with genotype-specific primers for determination of HCV genotypes 1a, 1b, 2a, 2b, 3a, 3b, 4, 5a, and 6a, as described previously (24).

PCR amplification of β-globin DNA. Total DNA was extracted from saliva samples using a QIAamp DNA Mini kit (QIAGEN) according to the manufacturer's instructions. To characterize the degree of cell contamination in saliva, isolated DNA was subsequently used as a template to amplify the human β-globin gene fragment of 268 bp with the following primers: 5′-GAA GAG CCA AGG ACA GGT AC-3′ and 5′-CAA CTT CAT CCA CGT TCA CC-3′ (21).

Statistical analysis. The Spearman rank test was used for evaluating the correlation between variables: anti-HCV antibody levels and viral loads in serum, saliva, and GCF.

RESULTS

The clinical and virological characteristics of 26 patients are presented in Table 1. The study group consisted of 10 males (38%) and 16 females (62%) with a mean age of 69 years (range, 56 to 79 years). Their mean liver enzyme values were as follows: 30 IU/liter for alanine aminotransferase (ALT) and 33 IU/liter for aspartic aminotransferase (AST). HCV RNA levels in the serum of 20 patients (77%) were determined by real-time RT-PCR assay, which showed a detection limit of 10^2 copies/ml and a linear range over 5 logs. Four of six serum samples whose HCV RNA levels were below the detection limit in this measurement were found to have detectable HCV RNA by the qualitative nested RT-PCR (4). We found no difference in efficiency and specificity of HCV cDNA amplification among genotypes 1b, 2a, and 2b in the real-time RT-PCR assay (data not shown).

Figure 1 summarizes viral loads in the serum, saliva, and GCF specimens of the patients. A mean serum HCV RNA level of 5.1×10^5 copies/ml was observed among samples with viral loads greater than 10^2 copies/ml. As expected, serum viral RNA levels were significantly correlated with anti-HCV antibody levels ($r = 0.80$, $P < 0.0001$) (Fig. 2A). In a number of cases (20 of 26; 77%), the viral load of the GCF was greater than that of the saliva. HCV RNA was detected in 31% of the saliva samples and 85% of the GCF specimens using real-time RT-PCR. Mean viral RNA levels were 1.9×10^4 (saliva) and 3.1×10^4 (GCF) copies/ml in these samples. It should be noted that most (seven out of eight) of the saliva samples contained 1.4×10^2 to 8.2×10^3 copies/ml of HCV RNA, with a mean value of 2.0×10^3 copies/ml among these seven samples (Fig. 1).

Among the 18 patients with HCV RNA-negative saliva, 10^2 to 10^3 copies/ml of viral RNA were detected in the GCF of 3 patients, 10^3 to 10^4 copies/ml of viral RNA were detected in the GCF of 2 patients, and $>10^4$ copies/ml were detected in

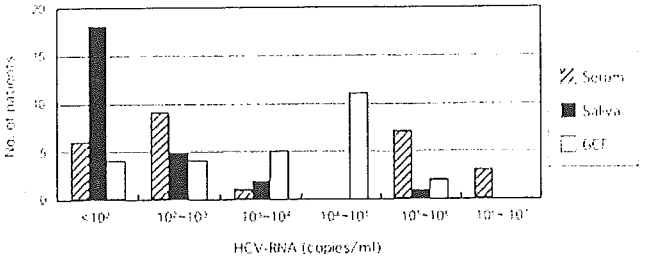

FIG. 1. HCV viral load in the serum, saliva, and GCF of anti-HCV-positive patients. Numbers of patients within each range of the viral load are indicated.

the GCF of 9 patients. No significant association was observed between viral RNA levels in the serum and viral RNA levels in the saliva (Fig. 2B) or GCF (Fig. 2C). However, relatively high serum viral loads ($>10^5$ copies/ml) were observed in five out of eight patients with HCV RNA-positive saliva, while serum viral loads were 1.5×10^3 copies/ml or less in most of the patients whose saliva specimens were negative (13 out of 18). Four patients with HCV RNA-positive saliva and/or GCF had no detectable serum HCV RNA by real-time RT-PCR (Fig. 2B and C); however, viral RNA was detectable in their sera by qualitative nested RT-PCR. Although no visible contamination of the saliva and GCF with blood was observed, there may be a small amount of cells or lysed cells in the fluids. To determine the degree of cell content in samples, total DNA was extracted from three saliva specimens, which contained $>10^3$ copies/ml of HCV RNA (Fig. 2B), and tested for the presence of cellular DNA by amplifying a human β-globin gene. A certain amount of cellular DNA was detectable in the saliva specimens (data not shown), suggesting some salivary HCV RNA may be derived from HCV-infected cells, such as BMC and mucosal epithelial cells, as discussed below. Various amounts of HCV-infected cells in the saliva and GCF may, in part, account for differences in the viral loads.

HCV RNA was detectable in most GCF and/or saliva specimens obtained from patients with clinical evidence of oral diseases: HCV RNA was detected in all 14 (100%) patients with periodontitis, 6 of 7 (85%) patients with squamous cell carcinoma, and 3 of 4 (75%) patients with lichen planus. Three out of four patients with HCV RNA-negative GCF, however, also had some oral epithelial lesions. On the other hand, among seven patients without oral diseases, HCV RNA was detected in the GCF and saliva of six and three patients, respectively. There was a trend toward increased viral loads in the oral fluids, especially GCF, among patients with bleeding on probing compared to those without the bleeding. The viral RNA levels in the GCF and saliva had no correlation with age, gender, or serum levels of ALT or AST. It also seems that their viral RNA levels were not correlated with HCV genotype, although the viral genotypes in 12 of 26 patients were not determined.

DISCUSSION

Identification of HCV in body fluids other than blood is important in order to evaluate possible nonparenteral routes of transmission. The role of oral fluids in HCV transmission remains controversial. Although the presence of HCV RNA in saliva has been reported by several research groups (6–11, 14, 17, 23, 25, 27, 29–33, 36–38), only one study has attempted to quantify HCV RNA in saliva, in which patients coinfected with HCV and human immunodeficiency virus were examined using a branched DNA assay (27). Moreover, limited information exists regarding the prevalence of HCV in the GCF of patients with hepatitis C, apart from one study in which a qualitative RT-PCR method was used to detect HCV in 59% of GCF and 35% of saliva specimens from patients with HCV viremia (20).

To the best of our knowledge, this study is the first to quantitate HCV loads within the saliva and GCF of anti-HCV antibody-positive patients using real-time RT-PCR. To search for a possible oral route of HCV transmission, whole saliva and GCF containing cell fractions were used to determine the viral

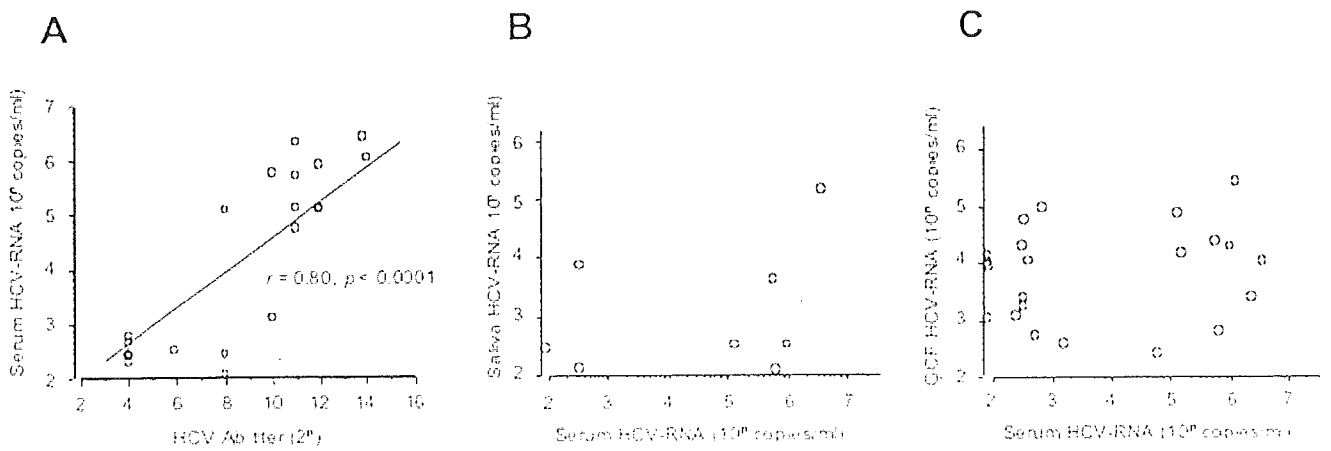

FIG. 2. (A) Correlation between anti-HCV antibody levels and HCV RNA levels in serum. The Spearman rank test was used for testing the correlation between variables. There is a significant positive correlation ($r = 0.80$, $P < 0.0001$) between the serum levels of HCV antibody detected by the passive hemagglutination assay and those of HCV RNA determined by real-time RT-PCR. (B) Correlation between viral loads in the serum and those in saliva specimens. Results for patients whose HCV RNA levels in saliva were $\geq 10^2$ copies/ml are plotted. No significant correlation was observed. (C) Correlation between viral loads in serum and those in GCF specimens. Results for patients whose HCV RNA levels in the GCF were $\geq 10^2$ copies/ml are plotted. No significant correlation was observed.

loads in this study. Although any saliva and GCF samples tested were not macroscopically observed to contain blood, we cannot rule out the possible effect of a small amount of bleeding as a source of HCV RNA. Here we observed HCV more commonly in the GCF than the saliva of HCV-seropositive patients. We further found viral loads of 10^2 to 10^4 copies/ml and 10^3 to 10^5 copies/ml in saliva and GCF, respectively. This result may be partially due to the presence of PCR inhibitors in saliva. An internal control to measure the possible effect of PCR inhibitors was not included in our real-time RT-PCR. Although the mean viral load within the GCF was approximately 10-fold lower than that in the serum, GCF samples from 12 of 26 patients (46%) had viral titers similar to or greater than those observed in the sera. No significant correlation was observed between the serum viremia levels and viral levels in the saliva or GCF. However, there was a trend that patients with HCV RNA-positive saliva showed higher viral loads in sera than patients with HCV RNA-negative saliva. These findings suggest that GCF might be one of the sources of HCV RNA within the saliva.

Although HCV is a hepatotropic virus, convincing evidence of HCV lymphotropism has been demonstrated in tissue culture (13). HCV has been widely detected in BMC in patients with chronic HCV infection, and differences in quasispecies identification within serum and BMC suggest that viral replication occurs within BMC (16, 22, 26, 28, 35, 38). HCV-infected BMC might allow HCV to infiltrate the GCF and saliva, since BMC migrate from dentogingival vessels into gingival crevices. There also might be transudation of HCV-containing serum into the mouth. Generally, periodontal inflammation increases the excretion of BMC-rich GCF. There is also a possibility that HCV exists within mucosal epithelial cells. HCV has been identified in the mucosal tissue, as well as salivary glands, of anti-HCV-positive patients with oral lichen planus using various techniques, including in situ hybridization, strand-specific RT-PCR, and immunohistochemistry (5, 32). Thus, it is likely that several possible sources discussed above are involved in HCV penetration into the saliva and GCF. Whatever the sources or mechanisms are, the findings obtained provide important implications for medical personnel regarding HCV transmission in health care settings as well as for HCV epidemiology, as the origin of the viral infection remains unclear in up to 40% of cases.

In this study, although the numbers of specimens were limited, we quantitatively determined HCV RNA in oral fluids from dental patients, including some patients with oral diseases, and demonstrated frequent detection of HCV in the saliva and GCF. Further large-scale epidemiological studies employing real-time RT-PCR assays are required to clarify the clinical significance of HCV in the saliva and GCF, including the potential for viral transmission through exposure to these fluids.

ACKNOWLEDGMENTS

We thank Yasushi Inoue and Ryosuke Suzuki for technical advice and helpful discussion on data analysis. We also thank Makiko Yahata for technical assistance and Tomoko Mizoguchi for manuscript preparation.

This work was partly supported by grants-in-aid from the Ministry of Health, Labor, and Welfare of Japan to T.S. and T.S.

REFERENCES

1. Abe, K., and G. Inchauspe. 1991. Transmission of hepatitis C by saliva. Lancet 337:248.
2. Aceti, A., G. Taliani, M. Sorice, and M. A. Amendolea. 1992. HCV and Sjogren's syndrome. Lancet 339:1425–1426.
3. Aizaki, H., K. J. Lee, V. M. Sung, H. Ishiko, and M. M. Lai. 2004. Characterization of the hepatitis C virus RNA replication complex associated with lipid rafts. Virology 324:450–461.
4. Aizaki, H., A. Saito, I. Kusakawa, Y. Ashiwara, S. Nagamori, G. Toda, T. Suzuki, K. Ishii, Y. Matsuura, and T. Miyamura. 1996. Mother-to-child transmission of a hepatitis C virus variant with an insertional mutation in its hypervariable region. J. Hepatol. 25:608–613.
5. Arrieta, J. J., E. Rodriguez-Inigo, N. Ortiz-Movilla, J. Bartolome, M. Pardo, F. Manzarbeitia, H. Oliva, D. M. Macias, and V. Carreno. 2001. In situ detection of hepatitis C virus RNA in salivary glands. Am. J. Pathol. 158: 259–264.
6. Chen, M., Z. B. Yun, M. Sallberg, R. Schvarcz, J. Bergquist, H. B. Berglund, and A. Sonnerborg. 1995. Detection of hepatitis C virus RNA in the cell fraction of saliva before and after oral surgery. J. Med. Virol. 45:223–226.
7. Couzigou, P., L. Richard, F. Dumas, L. Schouler, and H. Fleury. 1993. Detection of HCV-RNA in saliva of patients with chronic hepatitis C. Gut 34:S59–S60.
8. Fabris, P., D. Infantolino, M. R. Biasin, G. Marchelle, E. Venza, V. Terribile Wiel Marin, P. Benedetti, G. Tositti, V. Manfrin, and F. de Lalla. 1999. High prevalence of HCV-RNA in the saliva cell fraction of patients with chronic hepatitis C but no evidence of HCV transmission among sexual partners. Infection 27:86–91.
9. Fried, M. W., M. Shindo, T. L. Fong, P. C. Fox, J. H. Boofnagle, and A. M. Di Bisceglie. 1992. Absence of hepatitis C viral RNA from saliva and semen of patients with chronic hepatitis C. Gastroenterology 102:1306–1308.
10. Hermida, M., M. C. Ferreiro, S. Barral, R. Laredo, A. Castro, and P. Diz Dios. 2002. Detection of HCV RNA in saliva of patients with hepatitis C virus infection by using a highly sensitive test. J. Virol. Methods 101:29–35.
11. Hsu, H. H., T. L. Wright, D. Luba, M. Martin, S. M. Feinstone, G. Garcia, and H. B. Greenberg. 1991. Failure to detect hepatitis C virus genome in human secretions with the polymerase chain reaction. Hepatology 14:763–767.
12. Imhof, M., H. Popal, J. H. Lee, S. Zeuzem, and R. Milbradt. 1997. Prevalence of hepatitis C virus antibodies and evaluation of hepatitis C virus genotypes in patients with lichen planus. Dermatology 195:1–5.
13. Kato, N. 1999. Systems to culture hepatitis C virus, p. 261–278. *In* C. H. Hagedorn and C. M. Rice (ed.), The hepatitis C virus. Springer-Verlag, Berlin, Germany.
14. Komiyama, K., F. Kawamura, Y. Arakawa, H. Mastuo, N. Hayashi, T. Shikata, and I. Moro. 1995. Detection of hepatitis C virus (HCV)-RNA in saliva and gastric juice. Adv. Exp. Med. Biol. 371B:995–997.
15. Lee, S. C., A. Antony, N. Lee, J. Leibow, J. Q. Yang, S. Soviero, K. Gutekunst, and M. Rosenstraus. 2000. Improved version 2.0 qualitative and quantitative AMPLICOR reverse transcription-PCR tests for hepatitis C virus RNA: calibration to international units, enhanced genotype reactivity, and performance characteristics. J. Clin. Microbiol. 38:4171–4179.
16. Lerat, H., S. Rumin, F. Habersetzer, F. Berby, M. A. Trabaud, C. Trepo, and G. Inchauspe. 1998. In vivo tropism of hepatitis C virus genomic sequences in hematopoietic cells: influence of viral load, viral genotype, and cell phenotype. Blood 91:3841–3849.
17. Liou, T. C., T. T. Chang, K. C. Young, X. Z. Lin, C. Y. Lin, and H. L. Wu. 1992. Detection of HCV RNA in saliva, urine, seminal fluid, and ascites. J. Med. Virol. 37:197–202.
18. Lunel, F., and L. Musset. 1996. Hepatitis C virus infection and cryoglobulinemia. Viral Hepatitis Rev. 2:111–124.
19. Mariette, X., M. Zerbib, A. Jaccard, C. Schenmetzler, F. Danon, and J. P. Clauvel. 1993. Hepatitis C virus and Sjogren's syndrome. Arthritis Rheum. 36:280–281.
20. Maticic, M., M. Poljak, B. Kramar, K. Seme, V. Brinovec, J. Meglic-Volkar, B. Zakotnik, and U. Skaleric. 2001. Detection of hepatitis C virus RNA from gingival crevicular fluid and its relation to virus presence in saliva. J. Periodontol. 72:11–16.
21. McElhinney, L. M., R. J. Cooper, and D. J. Morris. 1995. Multiplex polymerase chain reaction for human herpesvirus-6, human cytomegalovirus, and human beta-globin DNA. J. Virol. Methods 53:223–233.
22. Muller, H. M., E. Pfaff, T. Goeser, B. Kallinowski, C. Solbach, and L. Theilmann. 1993. Peripheral blood leukocytes serve as a possible extrahepatic site for hepatitis C virus replication. J. Gen. Virol. 74:669–676.
23. Numata, N., H. Ohori, Y. Hayakawa, Y. Saitoh, A. Tsunoda, and A. Kanno. 1993. Demonstration of hepatitis C virus genome in saliva and urine of patients with type C hepatitis: usefulness of the single round polymerase chain reaction method for detection of the HCV genome. J. Med. Virol. 41:120–128.
24. Ohno, O., M. Mizokami, R. R. Wu, M. G. Saleh, K. Obba, E. Orito, M. Mukaide, R. Williams, and J. Y. Lau. 1997. New hepatitis C virus (HCV) genotyping system that allows for identification of HCV genotypes 1a, 1b, 2a, 2b, 3a, 3b, 4, 5a, and 6a. J. Clin. Microbiol. 35:201–207.